This indicated that the occurrence of insertion/deletion errors was considerably affected by the run conditions (probably due to variations in the absolute signal strengths of pyrosequencing). Thus, as previously reported, the detection of insertion/deletion mutations by MPS on the 454 GS-FLX system was quite error-prone at least at a limited number of residues. However, the results also implied that false-positive mosaic mutations could be avoided by considering the sequencing data for both strands because these run-dependent insertion/deletion errors occur only in a single strand. Taken together, we conclude that the obtained sequence error map is stable and sufficiently robust to discriminate substitution sequencing errors from low-level mosaicism.

3.2. *Discrimination formula for detection of somatic mosaicism with statistical confidence*

We next examined known SNPs, known heterozygous mutations and somatic mosaic mutations of CAPS patients using MPS. All of these variations appeared on both strands at the expected allele frequencies as shown in Fig. 2, again indicating that filtering the strand-specific sequence variations is unlikely to eliminate real genetic variations.

Based on the experimentally observed sequencing errors with the 454 GS-FLX system described above, we established a discrimination formula to detect low-level somatic mosaicism as follows. In previous studies, the number of reads with the sequence error of a certain category in a sequence position was modelled based on the Poisson distribution with two parameters λ and k where the expected number of reads containing an error and the observed number of reads containing a sequence alteration, respectively, are as shown below[18]:

$$\mathrm{Pois}(k;\lambda) = \frac{\lambda^k e^{-\lambda}}{k!}. \quad (1)$$

This model assumes that the error rate is constant across the different sequence regions but our data described above pointed out that the sequence error rate varies with the sequence content.[19] Thus, we introduced a position- and strand-specific error rate $q_{i,j,d}$ for a certain error category j in amplicon position i with strand d based on the sequencing data from 50 control samples. With the error rate $q_{i,j,d}$, the upper probability (P) that the number of reads (R) with a certain sequence alteration of category j in position i is equal or greater than the number of observed reads r out of N reads with a sequenced direction d for an unknown sample was defined as:

$$P(R \geq r_{i,j,d} | \lambda_{i,j,d}) = 1 - \sum_{k=0}^{r-1} \frac{\lambda_{i,j,d}^k e^{-\lambda_{i,j,d}}}{k!}, \quad (2)$$

where, $\lambda_{i,j,d} = N_{i,d} \times q_{i,j,d}$.

For the mismatch error rate, we did not consider the type of base substituted in an amplicon position in this study. We took $(1 - P)$ as a measure of the statistical confidence of the data and conventionally set a threshold of the statistical confidence to be 99.9%. In other words, if P-value was <0.001, the sequence alteration was considered to be a real sequence variation, not an error. For the final identification of real genetic variation with low-level somatic mosaicism, we determined that both of the P-values for the ith residue in the upper and lower strands must be smaller than the threshold.

To evaluate the lower detection limit for the allele frequencies of somatic mosaicism based on the statistical formulation shown above, we generated a series of known allele frequencies by diluting DNA from CAPS patients carrying heterozygous *NLRP3* mutations (c.1043C>T, c.1316C>T, and c.1985T>C) with DNA from normal donors carrying the wild-type *NLRP3* gene. In the dilution series, the mutant allele frequencies were adjusted to be 10, 5, 3, 2, 1, and 0.5% (Table 2). The data indicated that somatic mosaicism at these sites and at an allele frequency $\geq$1% could be convincingly detected with statistical significance ($P < 0.001$) if more than 350 reads for each strand were obtained for an amplicon. We also applied this statistical method to detect somatic mosaicism in patients with known low-level mosaic mutations described above and confirmed that all of

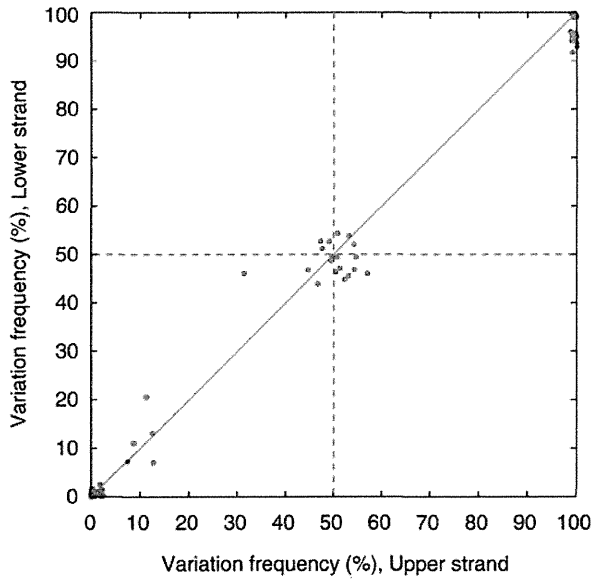

Figure 2. Scatter plot of the observed frequency variation in both strands. The colours depict known SNPs (green), heterozygous and mosaic mutations (orange) and errors (grey).

Table 2. Evaluation of the lower detection limit for mosaicism with three sets of dilution series

Mutation	Dilution (%)	Upper strand				Lower strand			
		Total reads	Mutant reads	%Mutant	*P*-value	Total reads	Mutant reads	%Mutant	*P*-value
c.1043C>T; p.Thr348Met	10.0	724	61	8.43	8.62E−130	520	57	10.96	1.73E−117
	5.0	453	24	5.30	2.86E−47	372	15	4.03	1.26E−25
	3.0	876	27	3.08	1.16E−46	757	21	2.77	6.83E−32
	2.0	737	10	1.36	1.05E−14	645	7	1.09	8.68E−09
	1.0	715	9	1.26	4.73E−13	624	4	0.64	1.11E−04
	0.5	1025	7	0.68	1.15E−14	756	3	0.40	3.22E−03[a]
c.1431C>A; p.Asn477Lys	10.0	542	65	11.99	1.22E−113	346	24	6.94	6.84E−49
	5.0	491	30	6.11	1.13E−44	356	17	4.78	2.42E−32
	3.0	487	21	4.31	1.26E−28	374	19	5.08	1.78E−36
	2.0	577	18	3.12	2.78E−22	495	9	1.82	4.57E−14
	1.0	491	4	0.82	9.17E−04	354	5	1.41	7.34E−08
	0.5	483	0	0	NA	424	3	0.71	NA
c.1985T>C; p.Met662Thr	10.0	658	79	12.01	1.13E−179	643	74	11.51	4.64E−167
	5.0	643	31	4.82	2.56E−59	608	33	5.43	9.96E−65
	3.0	777	27	3.48	4.65E−48	704	29	4.12	1.26E−53
	2.0	929	21	2.26	7.59E−34	835	15	1.80	3.92E−23
	1.0	735	17	1.09	2.74E−11	709	9	1.27	4.06E−13
	0.5	702	2	0.29	3.90E−03[a]	590	1	0.17	1.37E−01[a]

[a]Not significant.

Table 3. Potential mosaic mutations detected in patients with unknown mutations

Patient ID	Amplicon #	Variation		% Variation frequency		*P*-value		dbSNP	State
				Forward	Reverse	Forward	Reverse		
P1	Exon3_2	c.907G>C	p.Asp303His	7.12	11.56	3.0E−44	1.7E−84	rs121908153	Known
P2	Exon3_5	c.1699G>A	p.Glu567Lys	5.94	5.79	2.0E−69	8.9E−47	—	Known
P3	Exon3_5	c.1699G>A	p.Glu567Lys	18.28	15.33	0.0E+00	1.0E−312	—	Known
P4	Exon3_2	c.906C>A	p.Phe302Leu	9.78	9.70	1.7E−86	2.2E−122	—	Novel

the mutations could be detected with statistical significance without any false positives (data not shown).

3.3. *Detection and characterization of* NLRP3 *somatic mosaicism using the MPS platform*

To demonstrate the power of this approach in practice, we applied our new pipeline for 10 CINCA/NOMID patients in whom we failed to detect mutations in the *NLRP3* gene using a conventional direct DNA sequencing approach. The mutations detected by the analysis formulated using the MPS platform in this study are listed in Table 3. We successfully identified four out of the 10 patients with *NLRP3* somatic mosaicism, which was confirmed by subcloning and Sanger sequencing. The nucleotide substitutions were as follows (parentheses indicate the corresponding amino acid change): c.907G>C (p.Asp303His), c.1699G>A (p.Glu567Lys) in two patients, and c.906C>A (p.Phe302Leu). The frequencies of mosaicism identified in these patients by the MPS approach were consistent with those that were identified by the subcloning and subsequent capillary DNA sequencing method (data not shown). Both c.907G>C and c.1699G>A variants were reported as CINCA/NOMID-associated mutations in Infevers database (http://fmf.igh.cnrs.fr/ISSAID/infevers/) and in the dbSNP database (http://www.ncbi.nlm.nih.gov/projects/SNP/).[8]

Because the NLRP3 p.Phe302Leu mutation was novel and not detected in the 50 healthy controls, we performed an *in vitro* functional analysis to see the effect of p.Phe302Leu on the protein function. We used two different *in vitro* transfection experiments,

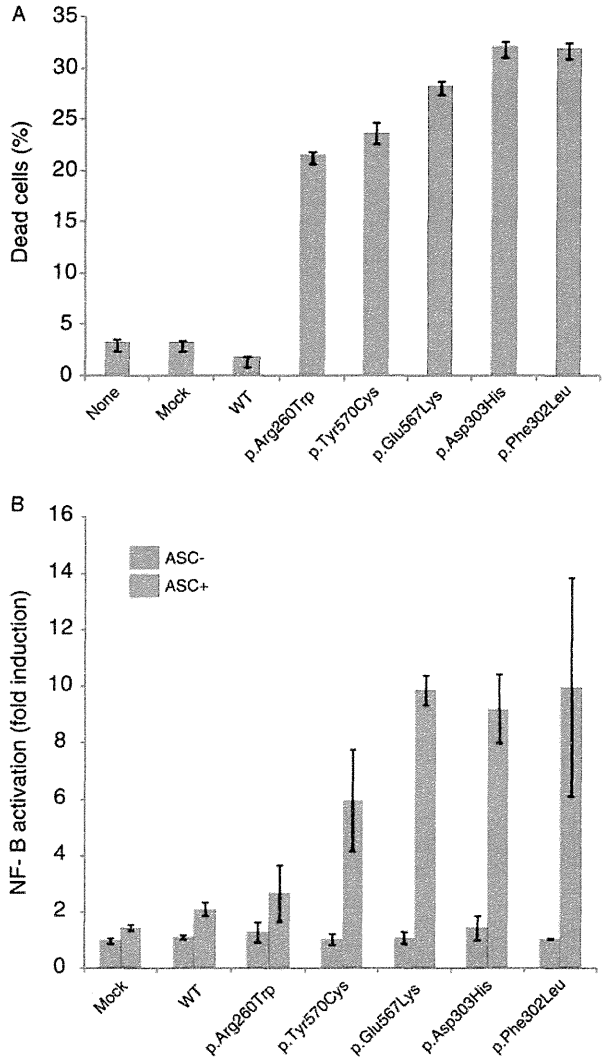

Figure 3. *In vitro* functional analysis of the identified *NLRP3* mosaic mutations. (A) Rapid cell death in transfected THP-1 cells. A GFP-fused wild-type or mutant *NLRP3* was transfected into THP-1 cells and incubated with PMA (10 ng/ml) for 4 h. The percentage of dead cells (7-amino-Actinomycin D [7-AAD]-positive) among the GFP-positive cells is shown. Data represent the means ± SD of triplicate experiments and are representative of two independent experiments. The data for previously reported mutations as well as the mutations found in this study are shown. (B) ACS-dependent NF-κB activation in transfected HEK293FT cells. HEK293FT cells were co-transfected with wild-type or mutant *NLRP3* in the presence or absence of ASC. NF-κB induction is shown as the fold-change compared with cells that were transfected with a control vector without ASC (set equal to one). Values are the means ± SD of triplicate experiments, and the data are representative of three independent experiments. The data for previously reported mutations (p.Arg260Trp and p.Tyr570Cys) and the mutations found in this study are shown. For each mutation, the data obtained in the presence and absence of ASC are shown. These findings identified p.Phe302Leu as a novel disease-causing mutation.

the rapid cell death in transfected THP-1 cells and the ASC-dependent NF-κB activation in transfected HEK293FT cells (Fig. 3A and B, respectively). Both assays clearly showed that p.Phe302Leu was a disease-causing mutation similar to known CINCA/NOMID-associated pathogenic mutations (p.Asp303His and p.Glu567Lys).[9]

4. Discussion

Although the somatic mutation rate at the nucleotide level *in vivo* was difficult to quantitatively measure due to the complexity of the genome and laborious molecular detection processes, recent advances in MPS technologies have allowed us to directly quantitate somatic mutations in human genome.[20–22] The current estimate for the somatic (*de novo*) mutation rate is $1-2 \times 10^{-8}$ residues/generation/haploid, and this estimate is sufficiently low that we would expect to never observe somatic mosaicism in the *NLRP3* gene by chance; although the error rate of the high-fidelity DNA polymerase used to produce the amplicons is two orders of magnitude larger than the somatic mutation rate,[23,24] we could not detect PCR-generated mosaicism higher than 1% in the 454 sequencing error maps. Based on the literature, the single base substitutions are the most frequent type of somatic mutations (~500 times more frequent than short insertions/deletions)[25] and protein-coding sequences are less mutagenic than sequences in non-coding regions, assuming that the somatic mutation spectrum in malignant cells is the same as in normal cells. Somatic mosaicism is thought to result from *de novo* gain-of-function-type mutations that are introduced at a very early and limited stage of development, and it is reasonable to focus our efforts on detecting base substitutions for somatic mosaicism in the *NLRP3* gene.

It is challenging but highly important in many areas of research, such as cancer, to detect low-level somatic mutations, which we designated as somatic mosaicism in this study, from apparently mutation-negative samples by conventional sequencing. Subcloning followed by the capillary DNA sequencing has been a *de facto* standard to identify somatic mosaicism, but this is not the method of choice for routine diagnostics because it is laborious, time consuming, and costly. Thus, it is reasonable for us to explore MPS as a new tool for this purpose. Although previous studies have used MPS technology to detect somatic mosaicism, it was unclear how sensitive this method is to detect a low-level somatic mosaicism using the MPS platform because this platform is generally error-prone. To address this challenge, we developed a new pipeline to detect low-level somatic mosaicism with statistical confidence using base position- and strand-specific error rate maps for the *NLRP3* amplicons to be studied. Whereas the

detection limit of somatic mosaicism depends on the base position and the read depth of the amplicons, the limit of detection could be as low as 1% allele frequency with no false positives for substitutions (the precision is higher than 99.9%). Our error map shows that 98.1% of base positions (3343 out of 3407 target positions) in the *NLRP3* exonic amplicons can be detected with ~1% mosaicism when more than ~350 reads were accumulated for each strand. Although the remaining region (64 base positions out of 3407 target positions) was too error-prone (the error rate ranged from 0.1 to 1.7% in either the upper or lower strand) to detect low-level mosaicism by MPS, medium-level mosaicism (5% or high) could be identified in all base positions in the target region with the same significance level. Based on this pipeline, we successfully identified four cases of somatic mosaicism among 10 apparently mutation-negative CINCA/NOMID patients. These results were subsequently confirmed by functional analysis and subcloning followed by capillary DNA sequencing method.

As described above, we revealed that a read depth of ~350 for each strand of each amplicon would be sufficient to detect somatic mosaicism as low as 1% with statistical confidence. This means that an analysis of somatic mosaicism (detection limit of 1% allele frequency) of the *NLRP3* gene for one sample requires $350 \times 2 \times 14 = 9800$ reads with the 454 GS-FLX sequencer, which has a capacity to obtain 1 000 000 reads per run. Thus, we could analyse ~100 patient samples with a single run (~10 h) using this MPS platform. For this purpose, a miniaturized 454 sequencer might be more convenient because it could analyse 10 patient samples at once with a reasonably reduced running cost.

The approach used to detect somatic mosaicism is very similar to that for low-frequency alleles in pooled DNA samples, for which MPS applications have been reported by many groups.[18,26,27] However, the main aim of these previous studies was to screen for a rare allele in a population. Thus, the discovery phase on the MPS platform must be followed by an evaluation phase using conventional methods. Therefore, when diagnosing somatic mosaicism of the *NLRP3* gene based solely on the MPS platform, we could not use the same approach to detect rare alleles in a population due to its low accuracy. The sequencing error rate on the Roche MPS platform was sufficiently stable and low enough as shown in this study. Using our pipeline, we were able to detect 1% somatic mosaicism in the *NLRP3* gene with 99.9% confidence. Although another research group recently used a similar approach with a short-read MPS,[28] the Roche long-read MPS is more suitable as a diagnostic tool mainly because of the short run time. If we could diagnose somatic mosaicism of the *NLRP3* gene within a reasonable time with low labour and costs as shown in this study, the success rate of CINCA/NOMID genetic diagnosis will increase from 60 to 80% or higher,[9] which will greatly advance the health and care of these patients and prevent irreversible bone and neurological complications of disease.

This pipeline would also be efficient to detect somatic mosaicism in mutation-negative patients with other diseases, including cancer. The error rate map for a given gene should be constructed from authentic plasmids, and used to detect somatic mosaicism of other genes as well as rare alleles in various populations.

Supplementary data: Supplementary data are available at www.dnaresearch.oxfordjournals.org.

Funding

This study was supported by the Japanese Ministry of Education, Science, Sports, and Culture, and the Japanese Ministry of Health, Labor, and Welfare.

Acknowledgements: We thank all patients who participated in the study. We are grateful to Ms. Yuki Takaoka at the Department of Pediatrics, Kyoto University Graduate School of Medicine and Mr. Takashi Watanabe at the Department of Human Genome Research, Kazusa DNA Research Institute for their technical assistance.

References

1. Prieur, A.M. and Griscelli, C. 1981, Arthropathy with rash, chronic meningitis, eye lesions, and mental retardation, *J. Pediatr.*, **99**, 79–83.
2. Hassink, S.G. and Goldsmith, D.P. 1983, Neonatal onset multisystem inflammatory disease, *Arthritis Rheum.*, **26**, 668–73.
3. Torbiak, R.P., Dent, P.B. and Cockshott, W.P. 1989, NOMID—a neonatal syndrome of multisystem inflammation, *Skeletal Radiol.*, **18**, 359–64.
4. Feldmann, J., Prieur, A.M., Quartier, P., et al. 2002, Chronic infantile neurological cutaneous and articular syndrome is caused by mutations in CIAS1, a gene highly expressed in polymorphonuclear cells and chondrocytes, *Am. J. Hum. Genet.* United States, 198–203.
5. Aksentijevich, I., Nowak, M., Mallah, M., et al. 2002, De novo CIAS1 mutations, cytokine activation, and evidence for genetic heterogeneity in patients with neonatal-onset multisystem inflammatory disease (NOMID)—a new member of the expanding family of pyrin-associated autoinflammatory diseases, *Arthritis Rheum.*, **46**, 3340–8.

6. Hoffman, H.M., Mueller, J.L., Broide, D.H., Wanderer, A.A. and Kolodner, R.D. 2001, Mutation of a new gene encoding a putative pyrin-like protein causes familial cold autoinflammatory syndrome and Muckle-Wells syndrome, *Nat. Genet.*, **29**, 301–5.
7. Goldbach-Mansky, R. 2011, Current status of understanding the pathogenesis and management of patients with NOMID/CINCA, *Curr. Rheumatol. Rep.*, **13**, 123–31.
8. Milhavet, F., Cuisset, L., Hoffman, H.M., et al. 2008, The infevers autoinflammatory mutation online registry: Update with new genes and functions, *Hum. Mutat.*, **29**, 803–8.
9. Tanaka, N., Izawa, K., Saito, M.K., et al. 2011, High incidence of NLRP3 somatic mosaicism in patients with chronic infantile neurologic, cutaneous, articular syndrome: results of an International Multicenter Collaborative Study, *Arthritis Rheum.*, **63**, 3625–32.
10. Qin, W., Kozlowski, P., Taillon, B.E., et al. 2010, Ultra deep sequencing detects a low rate of mosaic mutations in tuberous sclerosis complex, *Hum. Genet.*, **127**, 573–82.
11. Campbell, P.J., Pleasance, E.D., Stephens, P.J., et al. 2008, Subclonal phylogenetic structures in cancer revealed by ultra-deep sequencing, *Proc. Natl. Acad. Sci. USA*, **105**, 13081–6.
12. Rohlin, A., Wernersson, J., Engwall, Y., Wiklund, L., Bjoerk, J. and Nordling, M. 2009, Parallel sequencing used in detection of mosaic mutations: Comparison with four diagnostic DNA screening techniques, *Hum. Mutat.*, **30**, 1012–20.
13. Saito, M., Nishikomori, R., Kambe, N., et al. 2008, Disease-associated CIAS1 mutations induce monocyte death, revealing low-level mosaicism in mutation-negative cryopyrin-associated periodic syndrome patients, *Blood*, **111**, 2132–41.
14. Kent, W.J. 2002, BLAT—the BLAST-like alignment tool, *Genome Res.*, **12**, 656–64.
15. Fujisawa, A., Kambe, N., Saito, M., et al. 2007, Disease-associated mutations in CIAS1 induce cathepsin B-dependent rapid cell death of human THP-1 monocytic cells, *Blood*, **109**, 2903–11.
16. Gilles, A., Meglecz, E., Pech, N., Ferreira, S., Malausa, T. and Martin, J.F. 2011, Accuracy and quality assessment of 454 GS-FLX Titanium pyrosequencing, *BMC Genomics*, **12**, 245.
17. Margulies, M., Egholm, M., Altman, W.E., et al. 2005, Genome sequencing in microfabricated high-density picolitre reactors, *Nature*, **437**, 376–80.
18. Altmann, A., Weber, P., Quast, C., Rex-Haffner, M., Binder, E.B. and Muller-Myhsok, B. 2011, vipR: variant identification in pooled DNA using R, *Bioinformatics*, **27**, i77–84.
19. Dohm, J.C., Lottaz, C., Borodina, T. and Himmelbauer, H. 2008, Substantial biases in ultra-short read data sets from high-throughput DNA sequencing, *Nucleic Acids Res.*, **36**, e105.
20. Lee, W., Jiang, Z., Liu, J., et al. 2010, The mutation spectrum revealed by paired genome sequences from a lung cancer patient, *Nature*, **465**, 473–7.
21. Awadalla, P., Gauthier, J., Myers, R.A., et al. 2010, Direct Measure of the de novo mutation rate in Autism and Schizophrenia Cohorts, *Am. J. Hum. Genet.*, **87**, 316–24.
22. Conrad, D.F., Keebler, J.E.M., DePristo, M.A., et al. 2011, Variation in genome-wide mutation rates within and between human families, *Nat. Genet.*, **43**, 712–4.
23. Cha, R.S. and Thilly, W.G. 1993, Specificity, efficiency, and fidelity of PCR, *PCR Methods Appl.*, **3**, S18–29.
24. Vandenbroucke, I., Marck, H.V., Verhasselt, P., et al. 2011, Minor variant detection in amplicons using 454 massive parallel pyrosequencing: experiences and considerations for successful applications, *BioTechniques*, **51**, 167–77.
25. Pleasance, E.D., Cheetham, R.K., Stephens, P.J., et al. 2010, A comprehensive catalogue of somatic mutations from a human cancer genome, *Nature*, **463**, 191–6.
26. Fakhrai-Rad, H., Zheng, J.B., Willis, T.D., et al. 2004, SNP discovery in pooled samples with mismatch repair detection, *Genome Res.*, **14**, 1404–12.
27. Bansal, V. 2010, A statistical method for the detection of variants from next-generation resequencing of DNA pools, *Bioinformatics*, **26**, i318–24.
28. Flaherty, P., Natsoulis, G., Muralidharan, O., et al. 2012, Ultrasensitive detection of rare mutations using next-generation targeted resequencing, *Nucleic Acids Res.*, **40**, e2.

nature genetics

Genome-wide association study identifies eight new susceptibility loci for atopic dermatitis in the Japanese population

Tomomitsu Hirota[1], Atsushi Takahashi[2], Michiaki Kubo[3], Tatsuhiko Tsunoda[4], Kaori Tomita[5], Masafumi Sakashita[5], Takechiyo Yamada[5], Shigeharu Fujieda[5], Shota Tanaka[1,6], Satoru Doi[7], Akihiko Miyatake[8], Tadao Enomoto[9], Chiharu Nishiyama[10], Nobuhiro Nakano[10], Keiko Maeda[10], Ko Okumura[10], Hideoki Ogawa[10], Shigaku Ikeda[11], Emiko Noguchi[12,13], Tohru Sakamoto[14], Nobuyuki Hizawa[14], Koji Ebe[15], Hidehisa Saeki[16], Takashi Sasaki[17], Tamotsu Ebihara[17], Masayuki Amagai[17], Satoshi Takeuchi[18], Masutaka Furue[18], Yusuke Nakamura[19] & Mayumi Tamari[1]

Atopic dermatitis is a common inflammatory skin disease caused by interaction of genetic and environmental factors. On the basis of data from a genome-wide association study (GWAS) and a validation study comprising a total of 3,328 subjects with atopic dermatitis and 14,992 controls in the Japanese population, we report here 8 new susceptibility loci: *IL1RL1-IL18R1-IL18RAP* ($P_{combined} = 8.36 \times 10^{-18}$), the major histocompatibility complex (MHC) region ($P = 8.38 \times 10^{-20}$), *OR10A3-NLRP10* ($P = 1.54 \times 10^{-22}$), *GLB1* ($P = 2.77 \times 10^{-16}$), *CCDC80* ($P = 1.56 \times 10^{-19}$), *CARD11* ($P = 7.83 \times 10^{-9}$), *ZNF365* ($P = 5.85 \times 10^{-20}$) and *CYP24A1-PFDN4* ($P = 1.65 \times 10^{-8}$). We also replicated the associations of the *FLG*, *C11orf30*, *TMEM232-SLC25A46*, *TNFRSF6B-ZGPAT*, *OVOL1*, *ACTL9* and *KIF3A-IL13* loci that were previously reported in GWAS of European and Chinese individuals and a meta-analysis of GWAS for atopic dermatitis. These findings advance the understanding of the genetic basis of atopic dermatitis.

Atopic dermatitis is a chronic, relapsing skin disorder involving disturbed skin barrier functions, cutaneous inflammatory hypersensitivity and defects in antimicrobial immune defense with a strong genetic basis[1,2]. It is well established that common loss-of-function variants in *FLG* (encoding filaggrin) are a major predisposing factor for atopic dermatitis[3,4]. Association studies in populations of diverse ancestry, meta-analyses of studies and GWAS have shown that mutation in *FLG* is strongly associated with atopic dermatitis[4–7]. Apart from *FLG*, recent GWAS of European and Chinese populations for atopic dermatitis and a meta-analysis of GWAS have reported six susceptibility loci at a genome-wide level of significance—*C11orf30*, *TMEM232-SLC25A46*, *TNFRSF6B-ZGPAT*, *OVOL1*, *ACTL9* and *KIF3A-IL13*[5–7]. To gain a better understanding of the contribution of complex genetic effects to the pathogenesis of atopic dermatitis, it is important to identify additional susceptibility loci and validate the association of previously reported loci in different ancestry groups.

We performed a GWAS in the Japanese population with 1,472 individuals with atopic dermatitis (cases) and 7,971 controls using Illumina Human OmniExpress BeadChips (**Supplementary Table 1**). We subjected genotype data from a total of 606,164 SNPs to statistical analysis after principal-component analysis (PCA) and quality control filtering, and we generated a quantile-quantile plot using the Cochran-Armitage test (**Supplementary Fig. 1a–c**). The genomic inflation factor (λ_{GC}) was 1.03, indicating that there was a low possibility of false positive associations resulting from population stratification. The Manhattan plot showed that a total of 36 SNPs within 3 chromosomal regions at 2q12, 6p21.3 and 11p15.4 had associations that reached the genome-wide significance threshold of $P < 5 \times 10^{-8}$ (**Fig. 1**).

GWAS of European and Chinese populations and a meta-analysis of GWAS have reported seven susceptibly regions for atopic

[1]Laboratory for Respiratory Diseases, Center for Genomic Medicine, RIKEN, Yokohama, Japan. [2]Laboratory for Statistical Analysis, Center for Genomic Medicine, RIKEN, Minato-ku, Japan. [3]Laboratory for Genotyping Development, Center for Genomic Medicine, RIKEN, Yokohama, Japan. [4]Laboratory for Medical Informatics, Center for Genomic Medicine, RIKEN, Yokohama, Japan. [5]Department of Otorhinolaryngology, Fukui Medical University, Matsuoka, Japan. [6]Department of Otolaryngology–Head and Neck Surgery, University of Yamanashi, Faculty of Medicine, Chuo, Japan. [7]Osaka Prefectural Medical Center for Respiratory and Allergic Diseases, Habikino, Japan. [8]Miyatake Asthma Clinic, Osaka, Japan. [9]Nonprofit Organization (NPO) Japan Health Promotion Supporting Network, Wakayama, Japan. [10]Atopy Research Center, Juntendo University School of Medicine, Bunkyo-ku, Japan. [11]Department of Dermatology, Juntendo University School of Medicine, Bunkyo-ku, Japan. [12]Department of Medical Genetics, Majors of Medical Sciences, Graduate School of Comprehensive Human Sciences, University of Tsukuba, Tsukuba, Japan. [13]Japan Science and Technology Agency, Core Research for Evolutional Science and Technology (CREST), Saitama, Japan. [14]Division of Respiratory Medicine, Institute of Clinical Medicine, University of Tsukuba, Tsukuba, Japan. [15]Department of Dermatology, Takao Hospital, Kyoto, Japan. [16]Department of Dermatology, Jikei University School of Medicine, Minato-ku, Japan. [17]Department of Dermatology, Keio University School of Medicine, Shinjuku-ku, Japan. [18]Department of Dermatology, Graduate School of Medical Sciences, Kyushu University, Fukuoka, Japan. [19]Laboratory of Molecular Medicine, The Institute of Medical Science, The University of Tokyo, Minato-ku, Japan. Correspondence should be addressed to M.T. (tamari@src.riken.jp).

Received 27 April; accepted 11 September; published online 7 October 2012; doi:10.1038/ng.2438

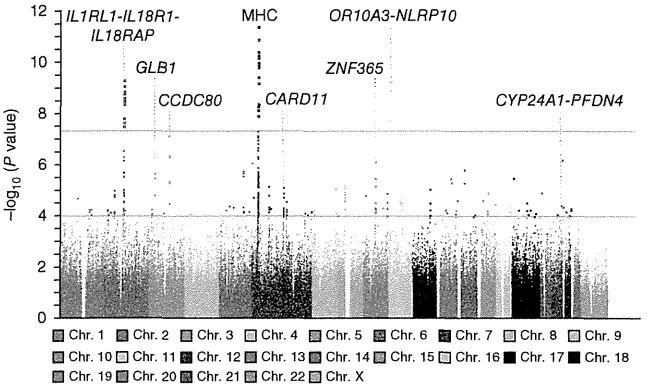

Figure 1 Manhattan plot showing the $-\log_{10} P$ values of 606,164 SNPs in the GWAS for 1,472 Japanese atopic dermatitis cases and 7,971 controls plotted against their respective positions on autosomes and the X chromosome. The red line shows the genome-wide significance threshold for this study ($P = 5 \times 10^{-8}$). The blue line shows the threshold ($P = 1 \times 10^{-4}$) for selecting SNPs for the validation study. Signals in the *IL1RL1-IL18R1-IL18RAP* (2q12), *GLB1* (3p21.33), *CCDC80* (3q13.2), MHC (6p21.3), *CARD11* (7p22), *ZNF365* (10q21.2), *OR10A3-NLRP10* (11p15.4) and *CYP24A1-PFDN4* (20q13) regions are indicated.

dermatitis[5–7]. We examined the previously reported regions in our GWAS and observed associations with atopic dermatitis for the SNPs in all of these regions (**Supplementary Fig. 2a–g** and **Supplementary Table 2**). Notably, the two regions identified in the previous GWAS of Chinese individuals had either the same SNP as the top signal in our study (20q13.3) or a SNP in strong linkage disequilibrium (LD) with the top SNP in the previous study (5q22.1); in contrast, for four of the five regions determined to be associated in Europeans, the top SNP in this study was in low LD with the previously reported best SNP.

To test for replication of the associations at the three loci suggested by the GWAS (2q12, 6p21.3 and 11p15.4) and to identify additional susceptibility loci for atopic dermatitis, we genotyped SNPs in a validation set consisting of a total of 1,856 individuals with atopic dermatitis and 7,021 controls (**Supplementary Table 1**). We first genotyped a total of ten tag SNPs ($r^2 < 0.80$) at the three loci and confirmed significant associations (**Supplementary Table 3**). We further investigated SNPs that showed P values of $<1 \times 10^{-4}$ in our GWAS and genotyped 87 tag SNPs ($r^2 < 0.80$) other than the previously reported loci and the three loci newly reported here. After Bonferroni correction with $P < 5.75 \times 10^{-4}$ (0.05/87), a total of 11 SNPs were found to be significantly associated with atopic dermatitis (**Supplementary Table 3**). We combined the data from the GWAS and

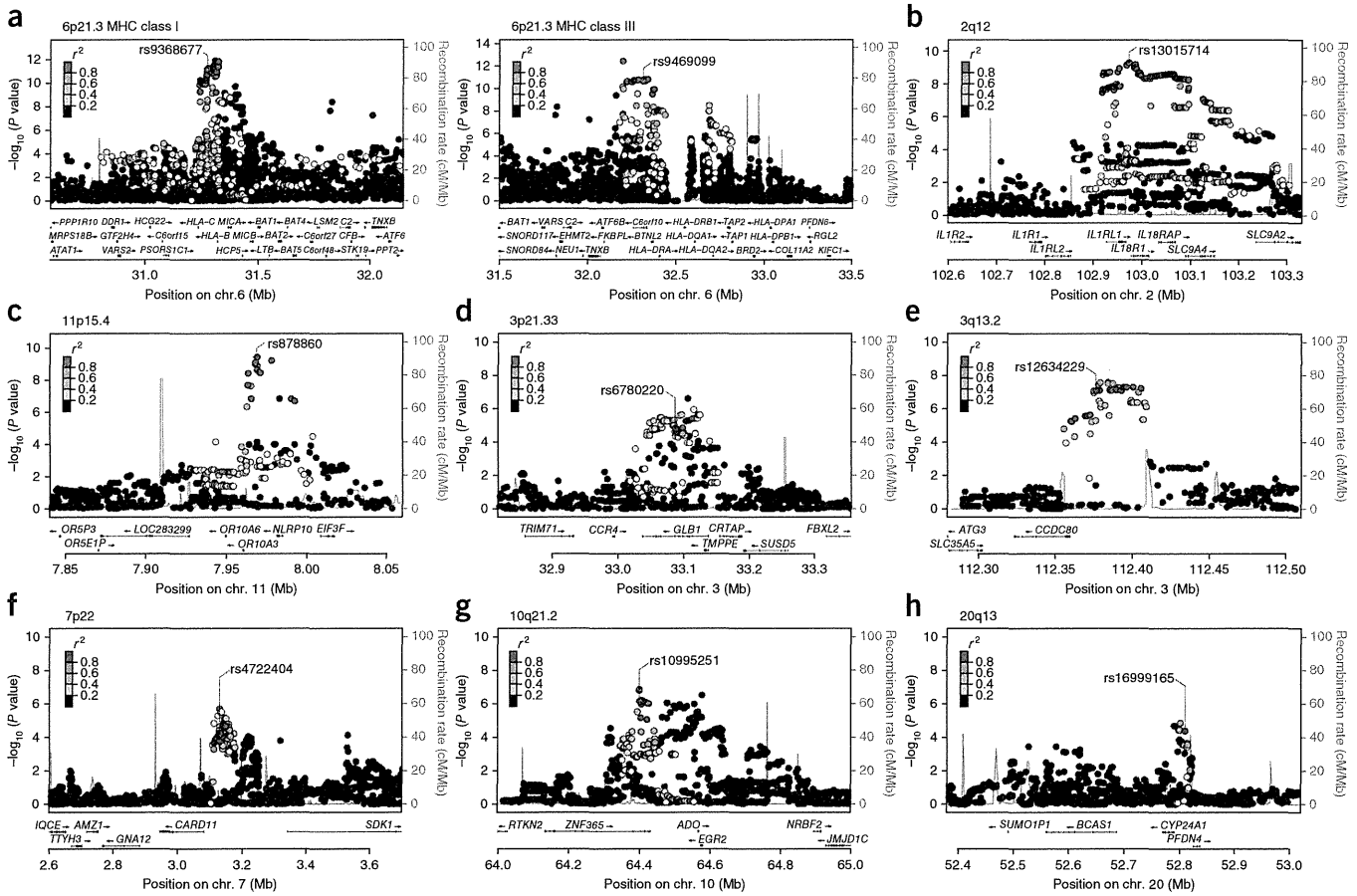

Figure 2 Regional plots of association results within eight newly identified susceptibility regions for atopic dermatitis. (**a–h**) Plots show the association results of both genotyped and imputed SNPs in the GWAS samples and the recombination rates within the susceptibility loci. For each plot, the $-\log_{10}$ P values (left y axis) of SNPs are shown according to their chromosomal positions (x axis). The genetic recombination rates are shown by the blue lines, and arrows indicate the locations of genes. The top genotyped SNP (labeled by rs number) is represented as a purple circle, and its LD (r^2) with the remaining SNPs is indicated by color. (**a**) MHC class I (left) and III (right) regions at 6p21.3. (**b**) 2q12. (**c**) 11p15.4. (**d**) 3p21.33. (**e**) 3q13.2. (**f**) 7p22. (**g**) 10q21.2. (**h**) 20q13.

Table 1 Summary of association results from the GWAS and validation study

SNP ID	Genes in or near regions of association	Chromosome (bp)	Allele (risk allele)	Stage	RAF		$P^{a,b}$	OR[b,c]	95% CI[b,c]	P_{het}[d]
					Case	Control				
rs13015714	*IL1RL1-IL18R1-IL18RAP*	2q12 (102971865)	T/G (G)	GWAS	0.473	0.412	5.17×10^{-10}	1.28	1.19–1.39	
				Validation	0.466	0.412	2.20×10^{-9}	1.25	1.16–1.34	
				Combined	0.470	0.412	8.36×10^{-18}	1.27	1.20–1.34	0.637
rs176095	*GPSM3* (MHC region)	6p21.3 (32158319)	T/C (T)	GWAS	0.860	0.811	3.86×10^{-10}	1.43	1.28–1.60	
				Validation	0.854	0.809	3.41×10^{-10}	1.38	1.25–1.53	
				Combined	0.856	0.810	8.38×10^{-20}	1.40	1.30–1.51	0.661
rs878860	*OR10A3-NLRP10*	11p15.4 (7968359)	A/G (G)	GWAS	0.603	0.540	3.47×10^{-10}	1.30	1.20–1.40	
				Validation	0.601	0.533	1.95×10^{-13}	1.32	1.23–1.42	
				Combined	0.602	0.537	1.54×10^{-22}	1.31	1.24–1.38	0.747
rs6780220	*GLB1*	3p21.33 (33087200)	T/G (G)	GWAS	0.582	0.539	1.55×10^{-5}	1.19	1.10–1.29	
				Validation	0.596	0.530	1.39×10^{-12}	1.31	1.21–1.41	
				Combined	0.590	0.535	2.77×10^{-16}	1.25	1.19–1.32	0.093
rs12634229	*CCDC80*	3q13.2 (112376308)	A/G (G)	GWAS	0.379	0.328	7.60×10^{-8}	1.25	1.15–1.36	
				Validation	0.391	0.326	8.18×10^{-14}	1.33	1.23–1.43	
				Combined	0.386	0.327	1.56×10^{-19}	1.29	1.22–1.37	0.303
rs4722404	*CARD11*	7p22 (3128789)	A/G (G)	GWAS	0.365	0.327	5.69×10^{-5}	1.18	1.09–1.28	
				Validation	0.362	0.325	2.67×10^{-5}	1.18	1.09–1.27	
				Combined	0.363	0.326	7.83×10^{-9}	1.18	1.12–1.25	0.911
rs10995251	*ZNF365*	10q21.2 (64398466)	T/C (C)	GWAS	0.568	0.518	7.73×10^{-7}	1.22	1.13–1.33	
				Validation	0.576	0.504	5.78×10^{-15}	1.34	1.24–1.44	
				Combined	0.572	0.511	5.85×10^{-20}	1.28	1.22–1.36	0.107
rs16999165	*CYP24A1-PFDN4*	20q13 (52807221)	T/C (T)	GWAS	0.729	0.691	3.87×10^{-5}	1.21	1.10–1.32	
				Validation	0.726	0.694	1.47×10^{-4}	1.17	1.08–1.27	
				Combined	0.728	0.692	1.65×10^{-8}	1.19	1.12–1.26	0.618

RAF, risk allele frequency; OR, odds ratio; CI, confidence interval.
[a]*P* values of the Cochran-Armitage trend test for each stage. [b]Results of combined analyses were calculated by the Mantel-Haenszel method. [c]Odds ratios and confidence intervals were calculated using the non-risk allele as a reference. [d]Results from the Breslow-Day test.

the validation set by the Mantel-Haenszel method, and a total of eight loci were found to be associated with atopic dermatitis at genome-wide significance (**Figs. 1** and **2** and **Table 1**). The Breslow-Day test showed an absence of significant heterogeneity ($P > 0.05$) (**Table 1**). We further assessed interactions among the eight newly discovered loci using the GWAS and validation data. We also conducted epistasis analysis, including the seven previously published loci, using the GWAS data. However, there was no evidence of an epistatic effect on susceptibility to atopic dermatitis with any combination of the 15 loci (**Supplementary Table 4**).

We obtained association results for >7 million imputed SNPs. In this study, a subset of genotype data for controls in the validation study was obtained from the GWAS data, but DNA samples were not available (**Supplementary Table 1**). Other cases and controls in the validation study were directly genotyped for SNPs at each locus. Thus, we focused on the directly genotyped SNPs in our GWAS and conducted a validation study. By imputation, we found that a total of 79 SNPs in 30 chromosomal regions were associated with atopic dermatitis at $5 \times 10^{-8} < P < 1 \times 10^{-4}$ (**Supplementary Table 5**). Further studies are needed to characterize the 30 regions suggested by imputation to associate with atopic dermatitis.

We next conducted conditional logistic regression analysis of the eight newly discovered loci using the GWAS data (**Supplementary Fig. 3**). This analysis indicated that there were two independent association signals in the MHC class I and III regions, one between *HLA-C* and *HLA-B* (rs9368677) and the other within *C6orf10* (rs9469099) (**Fig. 2a** and **Supplementary Fig. 3a**). In the *ZNF365* region, we observed independent signals at rs10995251, rs1444418 and rs10822056 (**Supplementary Fig. 3b**); however, the associations at rs1444418 and rs10822056 did not reach genome-wide significance when we combined the data from the GWAS and validation study ($P = 1.73 \times 10^{-7}$ and 1.15×10^{-4}, respectively). There were no independent signals in the other six associated regions (**Supplementary Fig. 3c–h**).

The associated region at 2q12 contains genes encoding the receptors of interleukin (IL)-1 family cytokines: *IL1RL1*, *IL18R1* and *IL18RAP* (**Fig. 2b** and **Table 1**). IL-1 family members are abundantly expressed in the skin[8]. IL1RL1, a component of the IL-33 receptor, is expressed by T helper type 2 (T_H2) cells and mast cells[9]. It has been reported that IL-33 is secreted in the damaged tissues of atopic dermatitis and promotes T_H2-type immune responses and the pathogenesis of atopic dermatitis[9]. The IL-1 receptor cluster region at 2q12 and the *IL33* region at 9p24.1 have also been identified as susceptibility loci by recent GWAS for bronchial asthma[10,11].

We found the most significant association with atopic dermatitis at rs176095 in the MHC class III region when we combined the data from the GWAS and validation study (**Fig. 2a** and **Table 1**). To our knowledge, this is the first finding of an association of atopic dermatitis with the MHC region at a genome-wide significance level. The MHC region is associated with a number of autoimmune diseases[12], and the involvement of autoimmunity in chronic inflammation in individuals with atopic dermatitis has been suggested[1]. Immunoglobulin E (IgE) antibodies against keratinocytes and endothelial cells are observed in serum specimens from subjects with severe atopic dermatitis[13].

The region of association at 11p15.4 includes two genes, *OR10A3* and *NLRP10* (**Fig. 2c** and **Table 1**). *OR10A3* is an olfactory receptor family gene, and *NLRP10* encodes a protein that belongs to the NALP protein family but lacks the leucine-rich repeat region. Individuals with atopic dermatitis are particularly susceptible to a number of microbial organisms, and pruritus is a major symptom of atopic dermatitis[1,2]. The itch-scratch cycle can lead to damage of the epidermal keratinocytes[1]. NLRP proteins are involved in sensing both microbial and danger signals[14], and NLRP10 has an anti-inflammatory

role through negative regulatory effects on caspase-1–dependent IL-1β secretion and apoptosis-associated speck-like protein containing a caspase recruitment domain (ASC)-mediated nuclear factor (NF)-κB activation[15].

The chromosome 3p21.33 region contains four genes, and the most significantly associated SNP, rs6780220, was located within *GLB1*, which encodes β-galactosidase-1 (**Fig. 2d** and **Table 1**). Notably, the associated region is located adjacent to the *CCR4* gene, which encodes a T_H2-associated chemokine receptor for CCL22 and CCL17 (also known as TARC). Keratinocyte-derived TSLP induces dendritic cells to produce TARC, and CCR4 mediates skin-specific recruitment of T cells during inflammation[1,16].

The associated region at 3q13.2 contains *CCDC80* (**Fig. 2e** and **Table 1**), which encodes a protein involved in the induction of C/EBPα and peroxisome proliferator-activated receptor γ (PPARγ)[17]. C/EBPα and C/EBPβ are coexpressed in basal keratinocytes and are upregulated when keratinocytes exit the basal layer and undergo terminal differentiation[18]. PPARγ acts as a negative regulator in immune cells, and a PPARγ agonist markedly suppresses both expression of thymic stromal lymphopoietin (TSLP) in the skin and maturation and migration of dendritic cells in a mouse model of atopic dermatitis[19].

The associated region at 7p22 contains *CARD11* (**Fig. 2f** and **Table 1**), which encodes CARMA1, an essential scaffold protein for lymphocyte activation via T-cell receptor (TCR) and B-cell receptor (BCR) signaling[20]. CARMA1 has an essential role in T-cell differentiation as well as a critical role in the regulation of the JunB and GATA3 transcription factors and the subsequent production of T_H2 cell–specific cytokines[21]. Mice that are homozygous for the mutation affecting Carma-1 show gradual development of atopic dermatitis with very high levels of serum IgE[22].

The region of association at 10q21.2 contains three genes, and the most significantly associated SNP, rs10995251, was located within *ZNF365* (**Fig. 2g** and **Table 1**). The region was reported to show suggestive association with atopic dermatitis ($P = 1.05 \times 10^{-7}$) by the previous GWAS of Chinese individuals[6], in which the association reached the genome-wide significance level. Notably, the region contains *EGR2*, which encodes a T-cell anergy-associated transcription factor that activates the expression of genes involved in the negative regulation of T-cell proliferation and inflammation[23].

The associated region at 20q13 includes *CYP24A1* and *PFDN4* (**Fig. 2h** and **Table 1**). *PFDN4* encodes a subunit of prefoldin, which is a molecular chaperone complex. *CYP24A1* encodes a mitochondrial cytochrome P450 superfamily enzyme. The protein initiates the degradation of 1,5-dihydroxyvitamin D3, the active form of vitamin D_3, by hydroxylation of the side chain[24]. Vitamin D is a modulator of innate and adaptive immune system functions[24], and an association between vitamin D deficiency and the severity of atopic dermatitis has been reported[25].

In this study, we identified variants at the *IL1RL1* and human leukocyte antigen (HLA) loci that associated with atopic dermatitis and replicated the associations at the *KIF3A-IL13* and *C11orf30* regions. The *C11orf30* region contains *LRRC32*, a gene previously reported to be specifically expressed in activated human naturally occurring regulatory T cells (nTreg)[26]. Atopic march is the natural history of atopic manifestations, and the clinical signs of atopic dermatitis generally predate the development of asthma and allergic rhinitis[27]. Recent GWAS have identified associations of the *IL1RL1*, HLA, *IL13* and *C11orf30* regions with bronchial asthma[10,11,28,29] and association of the *C11orf30* region with allergic rhinitis[30]. These findings suggest that atopic dermatitis and asthma or allergic rhinitis have overlapping susceptibility regions and that these regions contain common genetic factors for many allergic diseases. We stratified the cases by comorbidity of asthma and conducted an association study of asthma in the Japanese atopic dermatitis population for a total of 15 SNPs in the 7 previously reported and 8 newly identified regions. Notably, the most significant association was observed in the *IL1RL1* region ($P = 7.04 \times 10^{-9}$) (**Supplementary Table 6**).

In conclusion, we identified eight new susceptibility loci for atopic dermatitis at genome-wide significance, and we replicated the seven previously reported loci associated with atopic dermatitis in the Japanese population. Candidate genes at these loci suggest roles for epidermal barrier functions (*FLG* and *OVOL1*), adaptive immunity (*TNFRSF6B*, *IL13* and *CARD11*), IL-1 family signaling (*IL1RL1*, *IL18R1* and *IL18RAP*), negative regulation of apoptosis and the inflammatory response (*NALP10*), regulatory T cells (*LRRC32* and *EGR2*) and the vitamin D pathway (*CYP24A1*) in the pathogenesis of atopic dermatitis. Further studies are needed to better understand the genetic etiology and pathophysiology of atopic dermatitis.

URLs. The Leading Project for Personalized Medicine, http://biobankjp.org/; Haploview v4.2, http://www.broadinstitute.org/haploview/haploview; R statistical environment version 2.14.1, http://www.r-project.org/; minimac, http://genome.sph.umich.edu/wiki/Minimac; PLINK statistical software v1.07, http://pngu.mgh.harvard.edu/~purcell/plink/; LocusZoom, http://csg.sph.umich.edu/locuszoom/.

METHODS

Methods and any associated references are available in the online version of the paper.

Note: Supplementary information is available in the online version of the paper.

ACKNOWLEDGMENTS

We thank all the individuals who participated in the study and also thank the collaborating physicians for helping with sample collection. We are grateful to the members of BioBank Japan and the Rotary Club of Osaka-Midosuji District 2660 Rotary International in Japan for supporting our study. We thank M.T. Shimizu, H. Sekiguchi, A.I. Jodo, N. Kawaraichi and the technical staff of the Center for Genomic Medicine for providing technical assistance and K. Barrymore for proofreading this manuscript. This work was conducted as part of the BioBank Japan Project, which is supported by the Ministry of Education, Culture, Sports, Science and Technology, Japan. This work was also partly supported by grants from the Ministry of Health, Labour and Welfare, Japan.

AUTHOR CONTRIBUTIONS

T.H. and M.T. designed the study and drafted the manuscript. A.T. and T.T. analyzed the GWAS data. T.H., K.T., S. Tanaka and M.K. performed the genotyping for the GWAS. M.S., T.Y., S.F., S.D., A.M., T. Enomoto, C.N., N.N., K.M., S.I., K.O., H.O., E.N., T. Sakamoto, N.H., K.E., H.S., T. Sasaki, T. Ebihara, M.A., S. Takeuchi and M.F. recruited subjects and participated in the diagnostic evaluations. M.T. wrote the manuscript. M.K. and Y.N. contributed to the overall GWAS study design.

COMPETING FINANCIAL INTERESTS

The authors declare no competing financial interests.

Published online at http://www.nature.com/doifinder/10.1038/ng.2438.
Reprints and permissions information is available online at http://www.nature.com/reprints/index.html.

1. Bieber, T. Mechanisms of disease: atopic dermatitis. *N. Engl. J. Med.* **358**, 1483–1494 (2008).
2. Boguniewicz, M. & Leung, D.Y. Recent insights into atopic dermatitis and implications for management of infectious complications. *J. Allergy Clin. Immunol.* **125**, 4–13 (2010).
3. Palmer, C.N. *et al.* Common loss-of-function variants of the epidermal barrier protein filaggrin are a major predisposing factor for atopic dermatitis. *Nat. Genet.* **38**, 441–446 (2006).

4. Irvine, A.D., McLean, W.H. & Leung, D.Y. Filaggrin mutations associated with skin and allergic diseases. *N. Engl. J. Med.* **365**, 1315–1327 (2011).
5. Esparza-Gordillo, J. *et al.* A common variant on chromosome 11q13 is associated with atopic dermatitis. *Nat. Genet.* **41**, 596–601 (2009).
6. Sun, L.D. *et al.* Genome-wide association study identifies two new susceptibility loci for atopic dermatitis in the Chinese Han population. *Nat. Genet.* **43**, 690–694 (2011).
7. Paternoster, L. *et al.* Meta-analysis of genome-wide association studies identifies three new risk loci for atopic dermatitis. *Nat. Genet.* **44**, 187–192 (2012).
8. Johnston, A. *et al.* IL-1F5, -F6, -F8, and -F9: a novel IL-1 family signaling system that is active in psoriasis and promotes keratinocyte antimicrobial peptide expression. *J. Immunol.* **186**, 2613–2622 (2011).
9. Liew, F.Y., Pitman, N.I. & McInnes, I.B. Disease-associated functions of IL-33: the new kid in the IL-1 family. *Nat. Rev. Immunol.* **10**, 103–110 (2010).
10. Moffatt, M.F. *et al.* A large-scale, consortium-based genomewide association study of asthma. *N. Engl. J. Med.* **363**, 1211–1221 (2010).
11. Torgerson, D.G. *et al.* Meta-analysis of genome-wide association studies of asthma in ethnically diverse North American populations. *Nat. Genet.* **43**, 887–892 (2011).
12. Horton, R. *et al.* Gene map of the extended human MHC. *Nat. Rev. Genet.* **5**, 889–899 (2004).
13. Altrichter, S. *et al.* Serum IgE autoantibodies target keratinocytes in patients with atopic dermatitis. *J. Invest. Dermatol.* **128**, 2232–2239 (2008).
14. Magalhaes, J.G. *et al.* What is new with Nods? *Curr. Opin. Immunol.* **23**, 29–34 (2011).
15. Imamura, R. *et al.* Anti-inflammatory activity of PYNOD and its mechanism in humans and mice. *J. Immunol.* **184**, 5874–5884 (2010).
16. Vestergaard, C. *et al.* A Th2 chemokine, TARC, produced by keratinocytes may recruit CLA$^+$CCR4$^+$ lymphocytes into lesional atopic dermatitis skin. *J. Invest. Dermatol.* **115**, 640–646 (2000).
17. Tremblay, F. *et al.* Bidirectional modulation of adipogenesis by the secreted protein Ccdc80/DRO1/URB. *J. Biol. Chem.* **284**, 8136–8147 (2009).
18. Lopez, R.G. *et al.* C/EBPα and β couple interfollicular keratinocyte proliferation arrest to commitment and terminal differentiation. *Nat. Cell Biol.* **11**, 1181–1190 (2009).
19. Jung, K. *et al.* Peroxisome proliferator-activated receptor γ–mediated suppression of dendritic cell function prevents the onset of atopic dermatitis in NC/Tnd mice. *J. Allergy Clin. Immunol.* **127**, 420–429 (2011).
20. Hara, H. *et al.* Cell type–specific regulation of ITAM-mediated NF-κB activation by the adaptors, CARMA1 and CARD9. *J. Immunol.* **181**, 918–930 (2008).
21. Blonska, M. *et al.* CARMA1 controls Th2 cell–specific cytokine expression through regulating JunB and GATA3 transcription factors. *J. Immunol.* **188**, 3160–3168 (2012).
22. Jun, J.E. *et al.* Identifying the MAGUK protein Carma-1 as a central regulator of humoral immune responses and atopy by genome-wide mouse mutagenesis. *Immunity* **18**, 751–762 (2003).
23. Safford, M. *et al.* Egr-2 and Egr-3 are negative regulators of T cell activation. *Nat. Immunol.* **6**, 472–480 (2005).
24. Hart, P.H., Gorman, S. & Finlay-Jones, J.J. Modulation of the immune system by UV radiation: more than just the effects of vitamin D? *Nat. Rev. Immunol.* **11**, 584–596 (2011).
25. Peroni, D.G. *et al.* Correlation between serum 25–hydroxyvitamin D levels and severity of atopic dermatitis in children. *Br. J. Dermatol.* **164**, 1078–1082 (2011).
26. Wang, R. *et al.* Expression of GARP selectively identifies activated human FOXP3$^+$ regulatory T cells. *Proc. Natl. Acad. Sci. USA* **106**, 13439–13444 (2009).
27. Spergel, J.M. & Paller, A.S. Atopic dermatitis and the atopic march. *J. Allergy Clin. Immunol.* **112**, S118–S127 (2003).
28. Hirota, T. *et al.* Genome-wide association study identifies three new susceptibility loci for adult asthma in the Japanese population. *Nat. Genet.* **43**, 893–896 (2011).
29. Ferreira, M.A. *et al.* Identification of *IL6R* and chromosome 11q13.5 as risk loci for asthma. *Lancet* **378**, 1006–1014 (2011).
30. Ramasamy, A. *et al.* A genome-wide meta-analysis of genetic variants associated with allergic rhinitis and grass sensitization and their interaction with birth order. *J. Allergy Clin. Immunol.* **128**, 996–1005 (2011).

ONLINE METHODS

Study subjects. Characteristics of each case-control group are shown in **Supplementary Table 1**. All subjects with atopic dermatitis were diagnosed by physicians according to the criteria of Hanifin and Rajka[31]. All individuals were Japanese and gave written informed consent to participate in the study. This research project was approved by the ethical committees at the Institute of Medical Science, the University of Tokyo and the RIKEN Yokohama Institute.

BioBank Japan cases. The BioBank Japan project has been running since 2003, aiming at the collection of basic information for application to personalized medicine[32]. We selected case samples from the subjects who participated in the BioBank Japan, and a total of 1,472 cases for the GWAS and 940 cases for the validation study were recruited from several medical institutes, including the Fukujuji Hospital, Iizuka Hospital, Juntendo University, Hospital Iwate Medical University School of Medicine, National Hospital Organization Osaka National Hospital, Nihon University, Nippon Medical School, Shiga University of Medical Science, Cancer Institute Hospital of the Japanese Foundation for Cancer Research, Tokushukai Hospital and Tokyo Metropolitan Geriatric Hospital in Japan.

RIKEN cases. For the validation study, a total of 916 cases were recruited from the Takao Hospital, Kyushu University Hospital, University of Tokyo Hospital, Keio University Hospital, University of Tsukuba Hospital and several other hospitals.

BioBank controls. We used genome-wide screening data from subjects in the BioBank Japan project for the controls. Individuals with bronchial asthma and atopic dermatitis were excluded from the controls. Controls for the GWAS consisted of 6,042 cases in BioBank Japan with 1 of 5 diseases (cerebral aneurysm, esophageal cancer, endometrial cancer, chronic obstructive pulmonary disease and glaucoma), 1,023 healthy volunteers from members of the Rotary Club of Osaka-Midosuji District 2660 Rotary International in Japan[33] and 906 healthy subjects from the PharmaSNP Consortium.

A total of 5,547 cases registered in BioBank Japan with 1 of 4 diseases (epilepsy, urolithiasis, nephrotic syndrome and Graves' disease) were recruited for the validation study.

RIKEN controls. A total of 1,474 healthy volunteers were recruited from several medical institutes in Japan, including the Japanese Red Cross Wakayama Medical Center, Fukui University and Tsukuba University. Individuals with bronchial asthma and atopic dermatitis were excluded from the control group.

Genotyping and quality control. For the GWAS, we genotyped 1,491 cases and 7,983 controls using the Illumina Human OmniExpress BeadChip. We excluded a total of 19 cases and 12 controls because allele sharing analysis revealed that they were closely related, paired samples. We performed PCA of genotype data from the subjects along with data from European (CEU), African (YRI) and east Asian (Japanese (JPT) and Han Chinese (CHB) individuals obtained from the Phase 2 HapMap database by using smartpca[34]. The PCA plot indicated that cases and controls were genetically matched, with minimal evidence of population stratification (**Supplementary Fig. 1a,b**). We excluded samples with a call rate for autosomal SNPs of <0.98. We also excluded SNPs with minor allele frequencies of less than 0.01 from both cases and controls. SNPs having call rates of ≥99% in both cases and controls were used for the association study. We conducted exact Hardy-Weinberg equilibrium analysis, and SNPs with P values less than the cutoff value for the Hardy-Weinberg equilibrium test ($P < 1 \times 10^{-6}$ in controls) were excluded from the analysis.

In the validation study, we genotyped SNPs using the TaqMan assay (Life Technologies) or the multiplex PCR–based Invader assay (Third Wave Technologies). The genotype concordance rates for the eight SNPs in **Table 1** between samples genotyped using the Illumina Human OmniExpress BeadChip and those same samples genotyped with the TaqMan assay or multiplex PCR–based Invader assay were 1.000 and 1.000, respectively.

Statistical analysis. In the GWAS and validation study, the statistical significance of the association with each SNP was assessed using a 1-degree-of-freedom Cochran-Armitage trend test. We assessed association of SNPs on chromosome X by a meta-analysis with the Mantel-Haenszel method for two 2×2 allele frequency tables within male and female subjects. Odds ratios and confidence intervals were calculated from a 2×2 allele frequency table. We combined data from the GWAS and validation study by the Mantel-Haenszel method. Heterogeneity across the studies was examined using the Breslow-Day test[35]. Regional association plots were generated using LocusZoom[36].

Imputation. Imputation provides a high-resolution view of an associated region. Genotype imputation within the GWAS was performed using minimac. Association tests were performed with mach2dat using the fractional dosages output[37,38]. We used individuals from the 1000 Genomes Project (phased JPN, CHB and Han Chinese South (CHS) data, June 2011) as reference populations[39]. SNPs with a minor allele frequency of <5% and low quality of imputation ($r^2 < 0.7$) were excluded.

31. Hanifin, J.M. & Rajka, R.G. Diagnostic features of atopic dermatitis. *Acta Derm. (Stockholm)* **92** (suppl. 92), 44–47 (1980).
32. Nakamura, Y. The BioBank Japan Project. *Clin. Adv. Hematol. Oncol.* **5**, 696–697 (2007).
33. Takata, R. *et al.* Genome-wide association study identifies five new susceptibility loci for prostate cancer in the Japanese population. *Nat. Genet.* **42**, 751–754 (2010).
34. Price, A.L. *et al.* Principal components analysis corrects for stratification in genome-wide association studies. *Nat. Genet.* **38**, 904–909 (2006).
35. Breslow, N.E. & Day, N.E. Statistical methods in cancer research. Volume II—the design and analysis of cohort studies. *IARC Sci. Publ.* 1–406 (1987).
36. Pruim, R.J. *et al.* LocusZoom: regional visualization of genome-wide association scan results. *Bioinformatics* **26**, 2336–2337 (2010).
37. Li, Y. *et al.* MaCH: using sequence and genotype data to estimate haplotypes and unobserved genotypes. *Genet. Epidemiol.* **34**, 816–834 (2010).
38. Li, Y. *et al.* Genotype imputation. *Annu. Rev. Genomics Hum. Genet.* **10**, 387–406 (2009).
39. 1000 Genomes Project Consortium. A map of human genome variation from population-scale sequencing. *Nature* **467**, 1061–1073 (2010).

Immunity
Article

Inflammatory Monocytes Recruited to Allergic Skin Acquire an Anti-inflammatory M2 Phenotype via Basophil-Derived Interleukin-4

Mayumi Egawa,[1,6] Kaori Mukai,[1,4,6] Soichiro Yoshikawa,[1] Misako Iki,[1] Naofumi Mukaida,[3] Yohei Kawano,[1] Yoshiyuki Minegishi,[1,2,5] and Hajime Karasuyama[1,2,*]
[1]Department of Immune Regulation
[2]JST, CREST
Tokyo Medical and Dental University Graduate School of Medical and Dental Sciences, Tokyo 113-8519, Japan
[3]Division of Molecular Bioregulation, Cancer Research Institute, Kanazawa University, Kanazawa 920-1192, Japan
[4]Present address: Department of Pathology, Stanford University School of Medicine, Stanford, CA 94305, USA
[5]Present address: Department of Molecular Medicine, Institute for Genome Research, The University of Tokushima, Tokushima 770-8503, Japan
[6]These authors contributed equally to this work
*Correspondence: karasuyama.mbch@tmd.ac.jp
http://dx.doi.org/10.1016/j.immuni.2012.11.014

SUMMARY

Monocytes and macrophages are important effectors and regulators of inflammation, and both can be divided into distinct subsets based on their phenotypes. The developmental and functional relationship between individual subsets of monocytes and those of macrophages has not been fully elucidated, although Ly6C$^+$CCR2$^+$ inflammatory and Ly6C$^-$CCR2$^-$ resident monocytes are generally thought to differentiate into M1 (classically activated) and M2 (alternatively activated) macrophages, respectively. Here we show that inflammatory monocytes recruited to allergic skin acquired an M2-like phenotype in response to basophil-derived interleukin-4 (IL-4) and exerted an anti-inflammatory function. CCR2-deficient mice unexpectedly displayed an exacerbation rather than alleviation of allergic inflammation, in spite of impaired recruitment of inflammatory monocytes to skin lesions. Adoptive transfer of inflammatory monocytes from wild-type but not IL-4 receptor-deficient mice dampened the exacerbated inflammation in CCR2-deficient mice. Thus, inflammatory monocytes can be converted from being proinflammatory to anti-inflammatory under the influence of basophils in allergic reactions.

INTRODUCTION

Monocytes are circulating leukocytes that can differentiate into macrophages and dendritic cells after their migration to peripheral tissues (Auffray et al., 2009; Domínguez and Ardavín, 2010; Geissmann et al., 2010; Shi and Pamer, 2011). Monocytes, macrophages, and dendritic cells are essential components of the innate immune system and participate in clearance of dead cells and pathogens, tissue healing, and initiation and regulation of the adaptive immunity. They can also contribute to the pathogenesis of inflammatory disorders. Accumulating evidence indicates that those cell types can be further divided into phenotypically distinct subsets, and each subset might have particular function in the steady state and inflammation (Auffray et al., 2009; Geissmann et al., 2010; Gordon and Taylor, 2005; Mosser and Edwards, 2008; Shi and Pamer, 2011).

Circulating monocytes commonly express CD115 (CSF1 receptor) on their surface and are divided into subsets on the basis of the expression of particular surface molecules including chemokine receptors (Auffray et al., 2009; Gordon and Taylor, 2005). In humans, differential expression of CD14 and CD16 allowed monocytes to be divided into two subsets: CD14$^+$ CD16$^-$ and CD14$^+$CD16$^+$ monocytes (Passlick et al., 1989). The former cells represent 80%–90% of blood monocytes, express high amounts of the chemokine receptor CCR2 and low amounts of CX3CR1, and are often called classical monocytes. By contrast, the latter (nonclassical) cells express high amounts of CX3CR1 and low amounts of CCR2 and can be further divided into at least two populations based on the expression of CD14 and CD64. Also in mice, two subsets of monocytes have been described (Auffray et al., 2009; Geissmann et al., 2003). The main subset of murine monocytes expresses Ly6C, CCR2, and low amounts of CX3CR1, suggesting that they are phenotypically equivalent to human CD14$^+$CD16$^-$ monocytes. Ly6C$^+$CCR2$^+$ monocytes are readily recruited to affected tissues where they produce inflammatory cytokines such as tumor necrosis factor-α (TNF-α) and IL-1 during infection and inflammation, and they were therefore termed "inflammatory" monocytes. The second subset of murine monocytes is characterized by high expression of CX3CR1 and the lack of Ly6C and CCR2 expression and were termed "resident" monocytes because they have a longer half-life and are found in both resting and inflamed tissues. They adhere to and migrate along the luminal surface of endothelial cells that line small blood vessels and therefore appear to patrol the endothelium in the steady state (Auffray et al., 2007).

Macrophages are also heterogeneous in their phenotype and function, depending on the signals they receive (Biswas and

Mantovani, 2010; Gordon and Taylor, 2005; Mosser and Edwards, 2008; Murray and Wynn, 2011). Classically activated M1-type macrophages are generated by stimulation with bacterial moieties such as lipopolysaccharide (LPS) and the Th1 cell cytokine interferon-γ (IFN-γ), whereas alternatively activated M2-type macrophages are typically elicited by stimulation with the Th2 cell cytokines such as IL-4 and IL-13. M1 macrophages produce proinflammatory cytokines including IL-1 and destroy intracellular pathogens such as *M. tuberculosis* by means of an increased oxidative burst and NO production. Although the in vivo roles of M2 macrophages have been less well characterized, several functions are ascribed to them, including those in protection from parasitic infections, promoting Th2 cell-type immune responses, damping excessive inflammation, tumor progression, angiogenesis, wound healing, tissue remodeling, and fibrosis (Kreider et al., 2007; Martinez et al., 2009; Murray and Wynn, 2011).

The developmental and functional relationship between individual subsets of monocytes and those of macrophages has not been fully elucidated. It is generally thought that $Ly6C^+CCR2^+$ inflammatory monocytes exit the bone marrow in a CCR2-dependent manner and are recruited to inflamed tissues where they can differentiate to inflammatory M1 macrophages (Auffray et al., 2009; Dunay et al., 2008; Ingersoll et al., 2011; Serbina and Pamer, 2006; Tsou et al., 2007). In contrast, the differentiation of monocytes toward M2 macrophages remains ill defined. It has been suggested that $Ly6C^-CCR2^-$ resident monocytes are also recruited to sites of inflammation and then differentiate into M2 macrophages, contributing to wound healing (Auffray et al., 2007, 2009; Geissmann et al., 2010). Alternatively, recent study with a mouse model of helminth infection demonstrated that M2 macrophages are generated through IL-4-mediated proliferation and alternative activation of tissue-resident macrophages rather than the recruitment of blood monocytes (Jenkins et al., 2011). Thus, the origin of M2 macrophages and their mode of generation under homeostatic and pathological conditions remain obscure.

Basophils, the least common granulocyte, represent ~0.5% of peripheral blood leukocytes (Galli, 2000). Owing to their phenotypic similarities to mast cells and their small numbers, basophils had long been neglected in immunological studies. However, recent studies have defined previously unrecognized roles for basophils, including those in allergic responses, protection against parasitic infections, and regulation of acquired immunity (Karasuyama et al., 2011a; Min et al., 2012; Siracusa et al., 2011; Voehringer, 2011). Basophils readily generate large quantities of Th2 cell cytokines such as IL-4 and IL-13 (Piccinni et al., 1991; Seder et al., 1991), which contribute to initiation of Th2 cell differentiation (Perrigoue et al., 2009; Sokol et al., 2008, 2009; Yoshimoto et al., 2009) and to activation of B cells for the enhancement of humoral memory responses (Chen et al., 2009; Denzel et al., 2008). It remains to be investigated whether basophils and their products have any impact on the activation and differentiation of innate immune cells, including monocytes and macrophages.

In the present study, we analyzed the fate, polarization, and function of monocytes after their recruitment to skin lesions of immunoglobulin E (IgE)-mediated chronic allergic inflammation (IgE-CAI), a model where basophils rather than mast cells and T cells play a critical role for the elicitation of allergic response (Mukai et al., 2005). We found that $Ccr2^{-/-}$ mice unexpectedly displayed an exacerbation rather than alleviation of IgE-CAI, and ultimately identified a previously unappreciated mode of M2 generation, in that inflammatory monocytes can differentiate into anti-inflammatory M2-type macrophages via basophil-derived IL-4, which in turn dampen allergic inflammation.

RESULTS

$Ly6C^+CCR2^+$ Inflammatory Monocytes Are Recruited to Allergen-Exposed Skin in IgE-CAI

We previously showed that an intradermal administration of allergen induces three consecutive waves of ear swelling in mice sensitized with allergen-specific IgE, with peaks of swelling 30 min, 10 hr, and 3–4 days after the allergen challenge (Mukai et al., 2005). The delayed-onset (third) ear swelling with prominent inflammation was designated IgE-CAI (Mukai et al., 2005). Diphtheria toxin (DT)-mediated basophil ablation before the antigen challenge abolished the development of IgE-CAI in $Mcpt8^{DTR}$ mice (Wada et al., 2010) as shown in Figure 1A. This confirmed the conclusion in our previous studies that basophils play a pivotal role in the initiation of IgE-CAI, based on the results of experiments via the cell transfer and antibody-mediated basophil depletion (Mukai et al., 2005; Obata et al., 2007). Flow cytometric analysis revealed that the cell number in the skin lesions increased during the progress of IgE-CAI (Figure 1B). Monocyte- and macrophage-lineage cells (referred to here as monocytes-macrophages) and eosinophils were the major cell types among the cellular infiltrates whereas neutrophils and basophils were much less abundant (Figure 1C).

The vast majority of monocytes-macrophages isolated from the IgE-CAI skin lesions expressed Ly6C and CCR2, in contrast to those isolated from the control ear skin (Figure 2A and Figure S1A available online). Although resident macrophages in ear skin of naive mice barely express Ly6C, substantial numbers of $Ly6C^+CCR2^+$ monocytes-macrophages were detectable in the skin lesions even at 1 day after challenge (Figure S1A, top). These results suggested that monocytes-macrophages accumulating in the skin lesions were derived from $Ly6C^+CCR2^+$ inflammatory monocytes circulating in the peripheral blood (Figure S1B). Among the skin-infiltrating cells examined, basophils also expressed relatively high amounts of CCR2 on their surface in both C57BL/6 and BALB/c mice (Figure 2B). The expression of mRNAs encoding CCR2 ligands CCL8 and CCL12 (but not CCL2) was upregulated in the IgE-CAI skin lesions (Figure 2C). Various types of cells in the skin lesions expressed the CCR2 ligands, but basophils showed little or no expression of any of them (Figure S2A). Based on these observations, we assumed that CCR2 could contribute to the recruitment of both basophils and inflammatory monocytes to the skin lesions and hence the development of IgE-CAI.

$Ccr2^{-/-}$ Mice Show Exacerbated IgE-CAI in Spite of Impaired Recruitment of Inflammatory Monocytes

In sharp contrast to our expectation, the ear swelling in IgE-CAI was greatly augmented and prolonged in $Ccr2^{-/-}$ mice compared to that in wild-type mice (Figure 3A). Histopathological

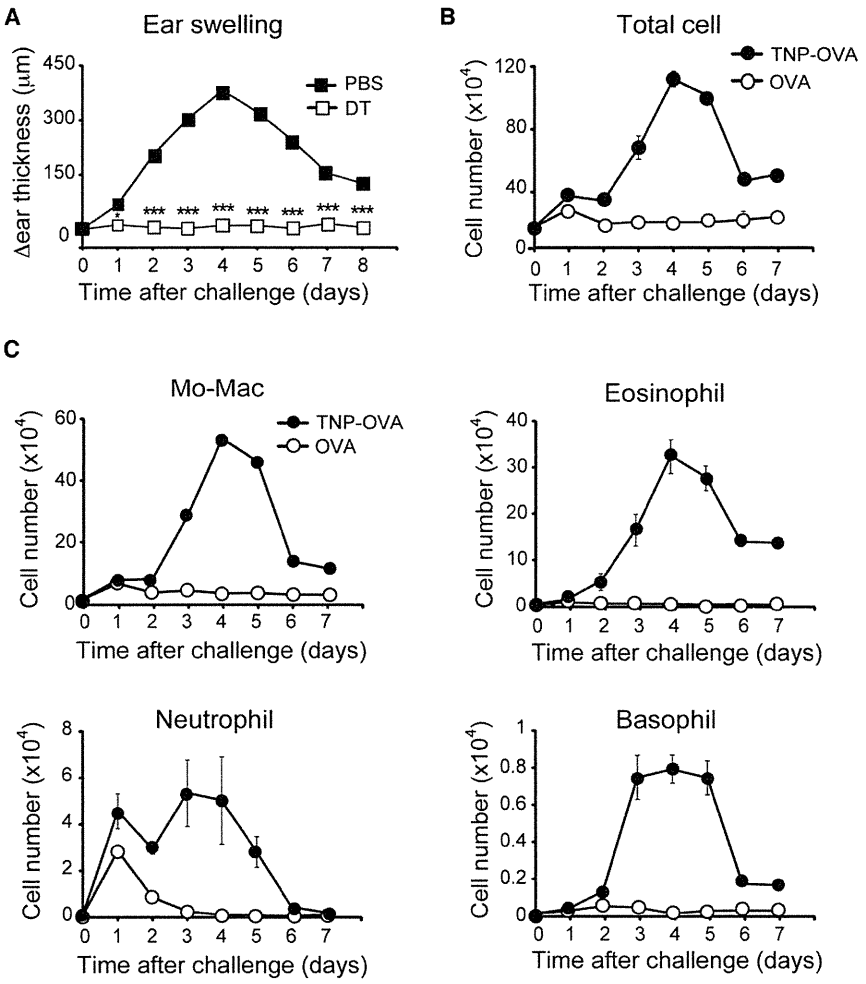

Figure 1. Cellular Components in the IgE-CAI Reaction that Is Elicited by Basophils

(A) *Mcpt8*^{DTR} C57BL/6 mice were sensitized with anti-TNP IgE and challenged with intradermal administration of TNP-OVA (or control OVA) in their ears to induce IgE-CAI. The mice were treated with either DT (open squares) or control PBS (closed squares) twice, 1 day before and 3 days after the antigen challenge. Time course of ear swelling (Δear thickness) is shown (mean ± SEM, n = 5 each). *p < 0.05, ***p < 0.001.

(B and C) C57BL/6 mice were sensitized with anti-TNP IgE and challenged with TNP-OVA (closed circles) or control OVA (open circles). The number of total cells (B) and indicated cell types (C) isolated from the ear skin at each time point postchallenge is shown (mean ± SEM, n = 3 each).

Data shown are representative of at least three independent experiments. Note that error bars are displayed in all figures, but often are hidden behind symbols such as squares and circles.

examination revealed many more cellular infiltrates in the skin lesion of *Ccr2*$^{-/-}$ mice (Figure 3B). Flow cytometric analysis demonstrated that the accumulation of monocytes-macrophages in the skin lesions was almost completely abolished in *Ccr2*$^{-/-}$ mice, as expected (Figure 3C). By contrast, the infiltration of basophils was enhanced rather than reduced in *Ccr2*$^{-/-}$ mice (Figure 3C), indicating that CCR2 was dispensable for the basophil recruitment, unlike for the monocyte recruitment. The accumulation of neutrophils in the skin lesions was also augmented in *Ccr2*$^{-/-}$ mice (Figure 3C). Thus, the IgE-CAI reaction was exacerbated rather than alleviated in *Ccr2*$^{-/-}$ mice, in spite of the fact that the recruitment of Ly6C^{+} inflammatory monocytes was abolished.

Monocytes-Macrophages in the Skin Lesions Display a Combined Phenotype of Inflammatory Monocytes and M2 Macrophages

To clarify the reason for this unexpected observation, we further examined the phenotype of monocytes-macrophages infiltrating the IgE-CAI skin lesions of wild-type mice. Approximately two-thirds of them expressed programmed death 1 ligand 2 (PD-L2) on their surface, whereas few cells isolated from the control skin did so (Figures 4A, 4B, and S1A, bottom). Because PD-L2 is a marker of M2-type macrophages (Loke and Allison, 2003), we examined the expression of other M2 markers in the skin lesions during the IgE-CAI reaction. The *Arg1*, *Chi3l3*, and *Fizz1* expression was upregulated and then downregulated, in parallel with the number of PD-L2^{+} monocytes-macrophages in the skin lesions (Figures 4B and 4C). Moreover, PD-L2^{+} monocytes-macrophages expressed significantly higher amounts of these mRNAs compared to PD-L2^{-} monocytes-macrophages and other cell lineages in the IgE-CAI skin lesions (Figures 4D and S2B), demonstrating that PD-L2^{+} monocytes-macrophages indeed displayed an M2 phenotype.

Gene profiling of monocytes-macrophages accumulating in the skin lesions revealed that M2 markers (*Arg1*, *Chi3l3*, and *Fizz1*) but not M1 markers (*Il1b*, *Nos2*, and *Tnfa*) were significantly upregulated during the IgE-CAI progression (Figure S3A). By contrast, the expression of the M2 markers and PD-L2 in blood monocytes, regardless of Ly6C expression, remained undetectable or very low during the IgE-CAI progression (Figures S3C and S3D). Importantly, the expression of genes involved in the macrophage differentiation (*Maf* and *Mafb*) but not those involved in the dendritic cell differentiation (*Sfpi1* and *Relb*) was upregulated in monocytes-macrophages in the skin lesions during the IgE-CAI progression (Figure S3B). These results strongly suggested that inflammatory monocytes recruited to the skin lesions differentiated into M2- but not M1-type macrophages during the IgE-CAI reaction. In contrast, monocytes-macrophages accumulating in skin lesions of delayed-type hypersensitivity (DTH) to the same antigen displayed an M1 phenotype with little or no expression of M2 markers including PD-L2 (Figure S4). Thus, the phenotype of monocytes-macrophages in skin lesions, either M1 or M2, appeared to be

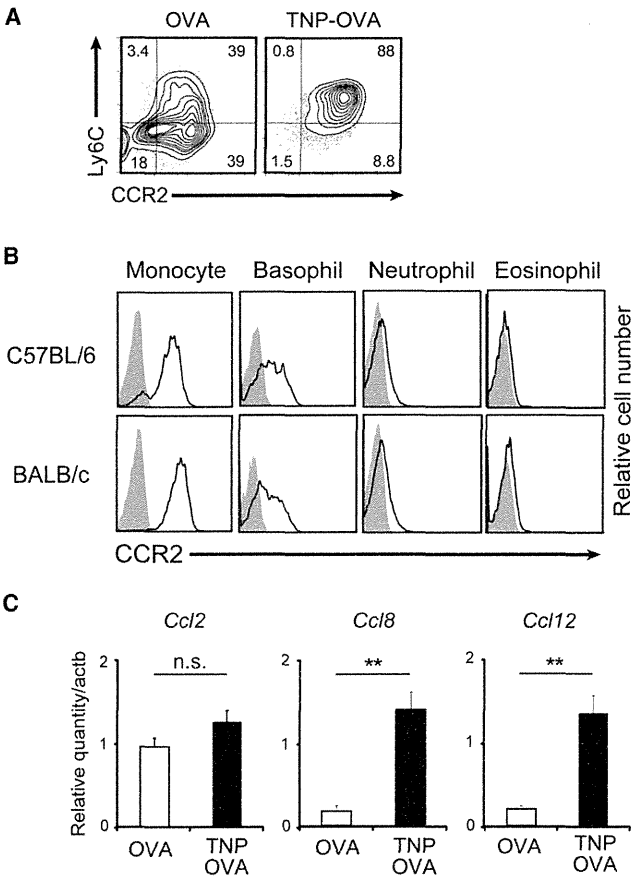

Figure 2. Monocytes-Macrophages Accumulating in the IgE-CAI Skin Lesions Display a Phenotype of Inflammatory Monocytes

(A) C57BL/6 mice were treated as in Figure 1 to induce IgE-CAI. The expression of Ly6C and CCR2 on F4/80$^+$CD11b$^+$SSC^{lo} monocytes-macrophages in the skin lesions of mice challenged with TNP-OVA or control OVA was examined on day 4 postchallenge.

(B) The expression of CCR2 on indicated cell lineages isolated from the bone marrow of C57BL/6 and BALB/c mice. Shaded histograms show control staining with isotype-matched antibody.

(C) The expression of indicated mRNAs in the skin lesions of mice challenged with TNP-OVA or control OVA was examined on day 3 postchallenge (mean ± SEM, n = 5 each).

Data shown are representative of three independent experiments. NS, not significant; **p < 0.01. See also Figures S1 and S2.

associated with the type of immune responses rather than the nature of antigens.

A previous study with a mouse model of helminth infection reported that M2 macrophages are generated through the proliferation and alternative activation of tissue-resident macrophages without any requirement of the blood monocyte recruitment (Jenkins et al., 2011). Therefore, we examined whether this mode of M2 generation could also take place in IgE-CAI. Although tissue-resident macrophages, mostly negative for Ly6C, were detected in ear skin of naive *Ccr2*$^{-/-}$ mice to an extent comparable to that observed in wild-type mice (Figure S5A), PD-L2$^+$ monocytes-macrophages were barely detected in the IgE-CAI skin lesions of *Ccr2*$^{-/-}$ mice (Figure 4E). Moreover, few monocytes-macrophages in the skin lesions of wild-type mice were positive for a proliferation marker Ki-67, regardless of the PD-L2 expression (Figure S5B). Thus, the proliferation and M2 conversion of tissue-resident macrophages appear to have little, if any, contribution to the M2 generation during the IgE-CAI reaction.

Basophil-Derived IL-4 Confers an M2-like Phenotype on Ly6C$^+$ Inflammatory Monocytes Ex Vivo

Th2 cell cytokines such as IL-4 and IL-13 as well as IL-10 have been shown to induce the differentiation of macrophages toward M2. Quantitative RT-PCR analysis revealed that the expression of *Il4* but not *Il13* or *Il10* mRNAs in the IgE-CAI skin lesions was upregulated in parallel with the accumulation of PD-L2$^+$ monocytes-macrophages (Figure 5A). *Il4* mRNAs were almost exclusively expressed by basophils among various cell types isolated from the skin lesions (Figure 5B). Indeed, primary basophils isolated from the bone marrow produced substantial amounts of IL-4 but not IL-13 when stimulated ex vivo with IgE plus antigens (Figure 5C).

Ly6C$^+$Ly6G$^-$ inflammatory monocytes freshly isolated from the bone marrow expressed no detectable PD-L2 on their surface (Figure 5D). Of note, they upregulated the PD-L2 expression when incubated ex vivo with the culture supernatants of primary basophils that had been stimulated with IgE plus antigens. This upregulation of PD-L2 was abolished when IL-4 antibody was included during the incubation (Figures 5D and 5E), indicating that basophil-derived IL-4 was responsible for the PD-L2 upregulation in inflammatory monocytes. The expression of *Arg1*, *Chi3l3*, and *Fizz1* mRNAs in inflammatory monocytes was also upregulated when incubated with the culture supernatants of activated basophils in an IL-4-dependent manner (Figure 5F). These results demonstrated that basophil-derived IL-4 can confer an M2-like phenotype on monocytes even before they differentiate into macrophages.

Skin-Infiltrating Monocytes Acquire an M2-like Phenotype in an IL-4R- and Basophil-Dependent Manner

We next examined whether the basophil IL-4-mediated acquisition of an M2-like phenotype by inflammatory monocytes indeed occurs in vivo. First, CD115$^+$ bone marrow monocytes were prepared from wild-type mice, labeled with CFSE, and adoptively transferred into IgE-sensitized wild-type mice, simultaneously with the challenge with allergens. On day 3 postchallenge, many of CFSE-labeled cells infiltrating the skin lesions became positive for PD-L2, concomitantly with F4/80 upregulation (Figure 6A), indicating their differentiation into M2-type macrophages. Of note, virtually all of the CFSE$^+$PD-L2$^+$F4/80$^+$ cells expressed Ly6C (Figure 6A), suggesting that they were derived from Ly6C$^+$ inflammatory but not Ly6C$^-$ resident monocytes. Indeed, when CD115$^+$Ly6C$^+$Ly6G$^-$ inflammatory monocytes were purified from the bone marrow and adoptively transferred, most of them became positive for PD-L2 in the skin lesions on day 3 postchallenge (Figure 6B).

Second, to examine the IL-4 dependency of M2 differentiation, CD115$^+$ bone marrow monocytes were prepared from wild-type or *Il4ra*$^{-/-}$ mice, labeled with CFSE, and adoptively transferred into wild-type mice, followed by IgE-CAI induction (Figure 6C). On day 1 postchallenge, when few basophils were recruited to the skin lesions (Figure 1C), little or no expression of PD-L2

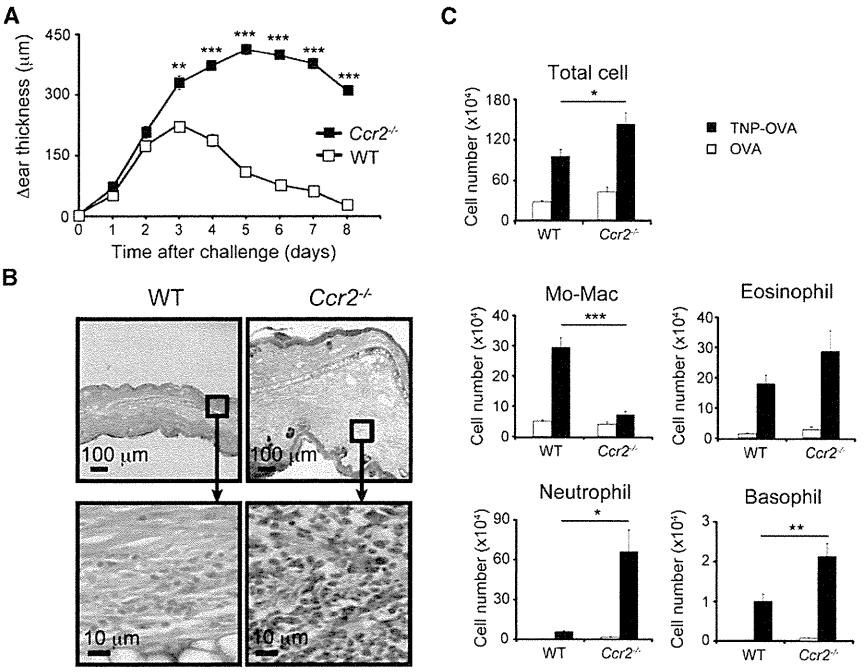

Figure 3. IgE-CAI Is Exacerbated rather than Ameliorated in *Ccr2*$^{-/-}$ Mice

Wild-type and *Ccr2*$^{-/-}$ BALB/c mice were treated as in Figure 1 to induce IgE-CAI.

(A) Time course of ear swelling (Δear thickness) in wild-type (open squares) and *Ccr2*$^{-/-}$ (closed squares) mice is shown (mean ± SEM, n = 4–5 each). Note that error bars are displayed, but often are hidden behind symbols.

(B) Giemsa-stained specimens of IgE-CAI skin lesions isolated 4 days postchallenge.

(C) The numbers of total cells and indicated cell types isolated from the ear skin on day 4 postchallenge are shown (mean ± SEM, n = 4–5 each). Data shown are representative of four independent experiments. *p < 0.05, **p < 0.01, ***p < 0.001.

was detected on CFSE-labeled cells infiltrating the skin lesions, regardless of the source of transferred cells (Figure 6C). On day 3 postchallenge, when the basophil infiltration reached a plateau (Figure 1C), a significant fraction of CFSE-labeled cells infiltrating the skin lesions expressed PD-L2 in mice that had received cells derived from wild-type but not *Il4ra*$^{-/-}$ mice (Figure 6C). Thus, monocytes recruited to the skin lesions acquired the PD-L2 expression in an IL-4 receptor (IL-4R)-dependent manner.

We then investigated whether basophils could contribute to this process. IgE-CAI was elicited in *Mcpt8*^{DTR} mice, and on day 2 postchallenge, CFSE-labeled CD115$^+$ bone marrow monocytes from wild-type mice were adoptively transferred to them, in conjunction with or without DT-mediated basophil ablation. The basophil ablation completely abolished the acquisition of PD-L2 expression by transferred monocytes infiltrating the skin lesions (Figure 6D). These results strongly suggested that blood-circulating monocytes acquire an M2-like phenotype after their recruitment to the IgE-CAI skin lesions, in response to basophil-derived IL-4.

Adoptive Transfer of Ly6C$^+$CCR2$^+$ Inflammatory Monocytes Dampens the Exacerbated IgE-CAI in *Ccr2*$^{-/-}$ Mice in an IL-4R-Dependent Manner

We next examined the functional consequence of the monocyte recruitment to the IgE-CAI skin lesions by means of adoptive transfer of wild-type monocytes to *Ccr2*$^{-/-}$ mice that display the exacerbated IgE-CAI. A single transfer of CD115$^+$ bone marrow monocytes at the time point of the antigen challenge, as shown in Figure 6A, showed no apparent impact on the ear swelling (data not show). We assumed that repeated transfer might be needed to reproduce the recruitment and accumulation of monocytes in the IgE-CAI skin lesions. Of note, four consecutive transfers of CD115$^+$ monocytes but not CD115$^-$ bone marrow cells dampened the exacerbated IgE-CAI in *Ccr2*$^{-/-}$ mice to the level observed in wild-type mice (Figure 7A), suggesting that CD115$^+$ bone marrow monocytes manifest an anti-inflammatory property after their recruitment to the skin lesion.

We then asked two questions. Are Ly6C$^+$Ly6G$^-$ inflammatory monocytes (rather than Ly6C$^-$ resident monocytes) that are recruited to and accumulate in the skin lesions indeed responsible for the negative regulation of IgE-CAI? Is the IL-4R-mediated acquisition of the M2-like phenotype by inflammatory monocytes associated with the regulation? To address these issues, Ly6C$^+$Ly6G$^-$ inflammatory monocytes were further purified from CD115$^+$ bone marrow cells, derived from either wild-type or *Il4ra*$^{-/-}$ mice, and directly transferred once into the ear dermis of *Ccr2*$^{-/-}$ mice where the antigens were administered (Figure 7B). The adoptive transfer of Ly6C$^+$Ly6G$^-$ inflammatory monocytes derived from wild-type but not *Il4ra*$^{-/-}$ mice dampened the exacerbated IgE-CAI. This strongly suggests that after the recruitment to the IgE-CAI skin lesions, CCR2$^+$Ly6C$^+$Ly6G$^-$ inflammatory monocytes acquired an M2-like phenotype through IL-4R and exerted an anti-inflammatory function to regulate the allergic inflammation.

DISCUSSION

Activated M2-type macrophages have been observed in a range of physiological and pathological processes, including Th2 cell-type immune responses (Kreider et al., 2007; Martinez et al., 2009; Murray and Wynn, 2011). However, the origin, differentiation pathway, and function of M2 macrophages have been ill defined, compared to those of M1 macrophages. In the present study, we have demonstrated a previously unappreciated cascade of monocyte-to-macrophage transition toward M2, being from proinflammatory to anti-inflammatory to dampen an allergic reaction. After recruitment to allergen-exposed skin, Ly6C$^+$CCR2$^+$ "inflammatory" monocytes acquired an M2-like phenotype and exerted an anti-inflammatory function in IgE-CAI, in response to IL-4 produced by antigen- and IgE-stimulated basophils. Accordingly, the failure in the recruitment

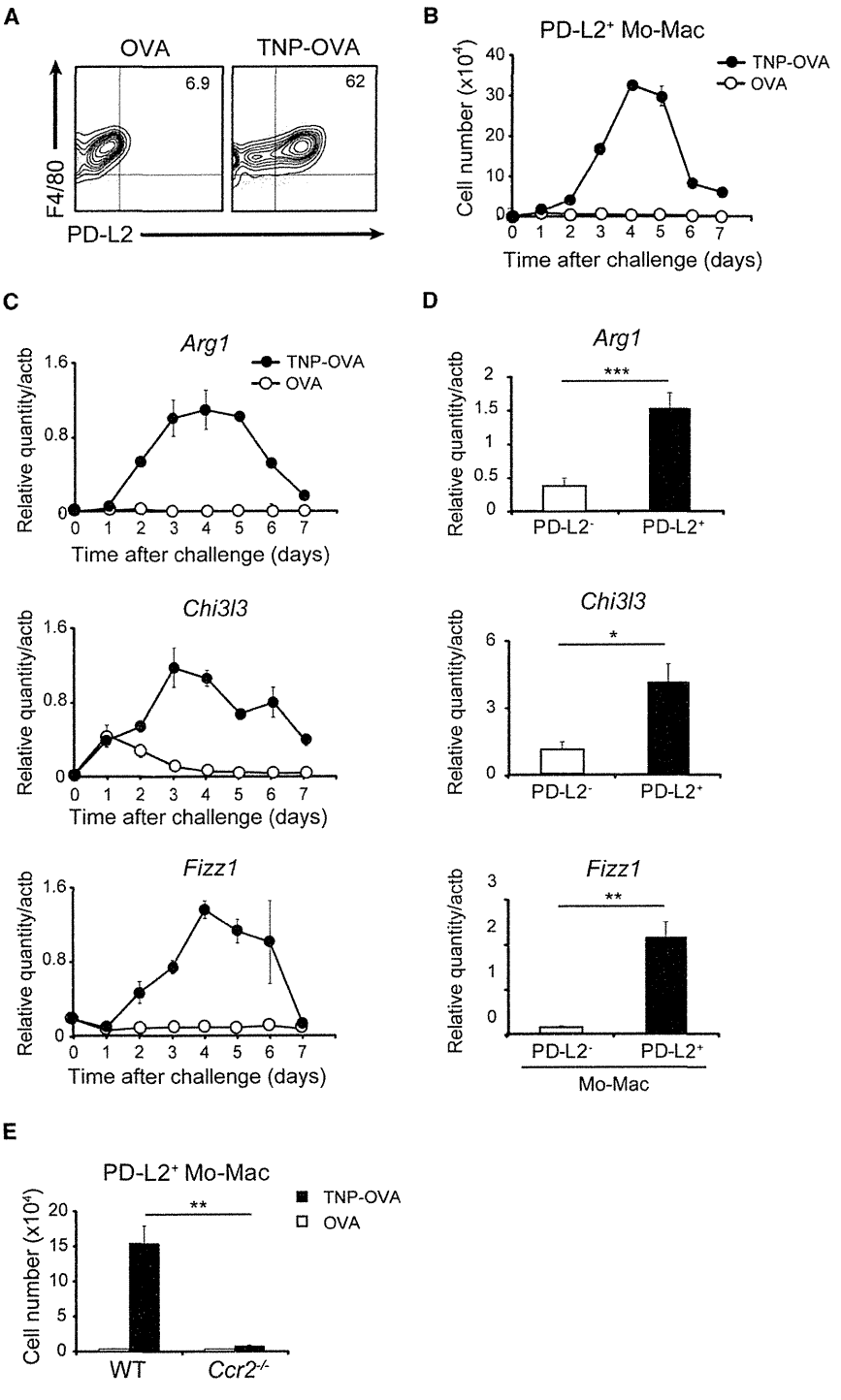

Figure 4. Monocytes-Macrophages Accumulating in the IgE-CAI Skin Lesions Display a Phenotype of M2-type Macrophages

(A–D) C57BL/6 mice were treated as in Figure 1 to induce IgE-CAI.

(A) The expression of PD-L2 on F4/80$^+$CD11b$^+$ SSC^{lo} monocytes-macrophages in the skin lesions of mice challenged with TNP-OVA or control OVA was examined on day 4 post-challenge.

(B and C) Time course of the PD-L2$^+$ monocytes-macrophage number (B, mean ± SEM, n = 3 each) and the expression of indicated mRNAs (C, mean ± SEM, n = 3 each) in the skin lesions of mice challenged with TNP-OVA (closed circles) or control OVA (open circles).

(D) The expression of indicated mRNAs in PD-L2$^-$ and PD-L2$^+$ monocytes-macrophages that were isolated on day 3 postchallenge from the ear skin of mice challenged with TNP-OVA (mean ± SEM, n = 6 each).

(E) Wild-type and *Ccr2*$^{-/-}$ BALB/c mice were treated as in Figure 3 to induce IgE-CAI. Data show the numbers of PD-L2$^+$ monocytes-macrophages that were isolated on day 4 postchallenge from the ear skin of mice challenged with TNP-OVA or control OVA (mean ± SEM, n = 4–5 each). Data shown are representative of at least three independent experiments. *p < 0.05, **p < 0.01, ***p < 0.001. See also Figures S1–S5.

of inflammatory monocytes in *Ccr2*$^{-/-}$ mice resulted in the exacerbation rather than alleviation of allergic inflammation, and adoptive transfer of CCR2$^+$ inflammatory monocytes normalized it. Thus, M2-like monocytes-macrophages derived from inflammatory monocytes appear to negatively regulate allergic inflammation in IgE-CAI.

Previous studies have shown two distinct modes of M2 generation. One is based on the observation during infection with *Listeria monocytogenes*. Ly6C$^{lo/-}$ resident monocytes recruited to the infection site turn on the expression of typical M2 marker genes, including *Arg1* and *Fizz1*, indicating their differentiation into M2 macrophages that probably contribute to tissue repair (Auffray et al., 2007). In contrast, Ly6C$^+$ inflammatory monocytes differentiate into dendritic cells that produce inflammatory mediators (Kurihara et al., 1997; Serbina et al., 2003). The other mode of M2 generation has been demonstrated in infection with helminth *Litomosoides sigmodontis*, in that M2 macrophages are generated through proliferation and alternative activation of tissue-resident macrophages rather than the recruitment of circulating monocytes (Jenkins et al., 2011). Our study on IgE-CAI has identified the third mode of M2 generation, in that Ly6C$^+$ inflammatory monocytes give rise to M2-type macrophages. The differentiation of inflammatory monocytes to M2 macrophages may not be restricted to allergic responses. A similar differentiation was suggested in experimental autoimmune encephalomyelitis, even though no direct evidence for this in vivo was provided (Denney et al., 2012).

The in vivo function of M2 macrophages has been less well characterized, compared to that of M1 macrophages, but has

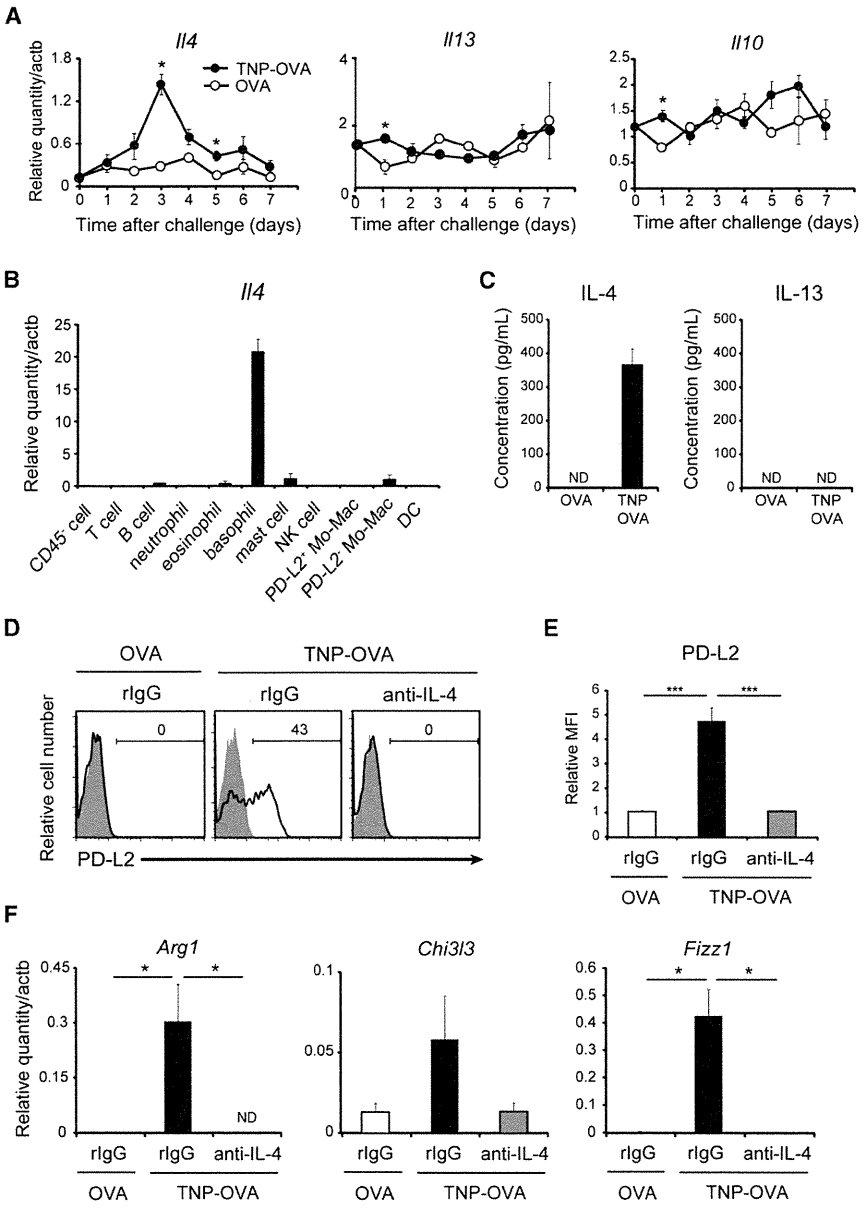

Figure 5. Basophil-Derived IL-4 Confers an M2-type Phenotype on Ly6C$^+$ Inflammatory Monocytes Ex Vivo

(A and B) C57BL/6 mice were treated as in Figure 1 to induce IgE-CAI. Time course of the expression of indicated mRNAs in the skin lesions of mice challenged with TNP-OVA (closed circles) or control OVA (open circles) is shown in (A) (mean ± SEM, n = 3 each). *p < 0.05. In (B), the indicated cell lineages were isolated on day 3 postchallenge from the skin lesions of mice challenged with TNP-OVA and subjected to quantitative RT-PCR for the analysis of *Il4* expression (mean ± SEM, n = 3 each).

(C) Basophils (2 × 10^5 cells/ml) enriched from bone marrow cells were sensitized ex vivo with anti-TNP IgE and then stimulated with TNP-OVA or control OVA at 37°C for 10 hr, and the concentration of IL-4 and IL-13 in their culture supernatants was determined by ELISA (mean ± SEM, n = 5 each). ND, not detectable.

(D–F) Ly6C$^+$ inflammatory monocytes were purified from C57BL/6 bone marrow cells and incubated at 37°C for 24 hr in the presence of anti-IL-4 or control rat IgG (rIgG), with the culture supernatants of basophils that had been stimulated as in (C).

(D and E) The cultured monocytes were subjected to flow cytometric analysis for PD-L2 expression. Representative staining profiles are shown in (D). Shaded histograms show control staining with isotype-matched antibody. All the data are summarized in (E) (mean ± SEM, n = 5–7 each), in that the relative mean fluorescence intensity (MFI) was calculated as MFI (PD-L2 staining)/MFI (control staining).

(F) The cultured monocytes were subjected to quantitative RT-PCR analysis for expression of indicated mRNAs (mean ± SEM, n = 5 each).

Data shown are representative of at least three independent experiments. *p < 0.05, ***p < 0.001.

been implicated in a variety of processes, including protection against parasitic infection, promoting Th2 cell-type immune responses, wound healing, tissue fibrosis, metabolic regulation, angiogenesis, and tumorigenesis (Kreider et al., 2007; Martinez et al., 2009; Murray and Wynn, 2011). The role of M2 macrophages in allergy and asthma has not been well understood, in contrast to the extensive study on its role in parasitic infections. Of note, in mice infected with helminth *Schistosoma mansoni*, M2 macrophages and their products have been shown to suppress rather than promote Th2 cell-type inflammation (Nair et al., 2009; Pesce et al., 2009). No such anti-inflammatory property of M2 macrophages was definitely demonstrated in allergic responses, as far as we aware. Instead, in mouse models of airway allergic inflammation, M2 macrophages reportedly contribute to the pathogenesis of disease, including promotion of inflammation (Ford et al., 2012; Kim et al., 2008; Kurowska-Stolarska et al., 2009; Melgert et al., 2010; Moreira et al., 2010; Nagarkar et al., 2010) and angiogenesis (Sun et al., 2008). Intriguingly, *Ccr2*$^{-/-}$ mice were reported to display enhanced airway allergic inflammation, but the underlying mechanism remains to be determined (Kim et al., 2001).

In the present study, we clearly demonstrated that M2-like monocytes-macrophages derived from inflammatory monocytes exert an anti-inflammatory function in IgE-CAI. Their absence or the failure in their conversion to M2 type resulted in the exacerbation of allergic inflammation. Thus, M2-like monocytes-macrophages appear to dampen excessive inflammation in IgE-CAI. It remains to be definitely demonstrated how they exert an anti-inflammatory function. Treatment of mice with an inhibitor of arginase-1 showed no apparent effect on IgE-CAI (data not show), although arginase-1 has been shown to suppress Th2 cell-type inflammation in helminth

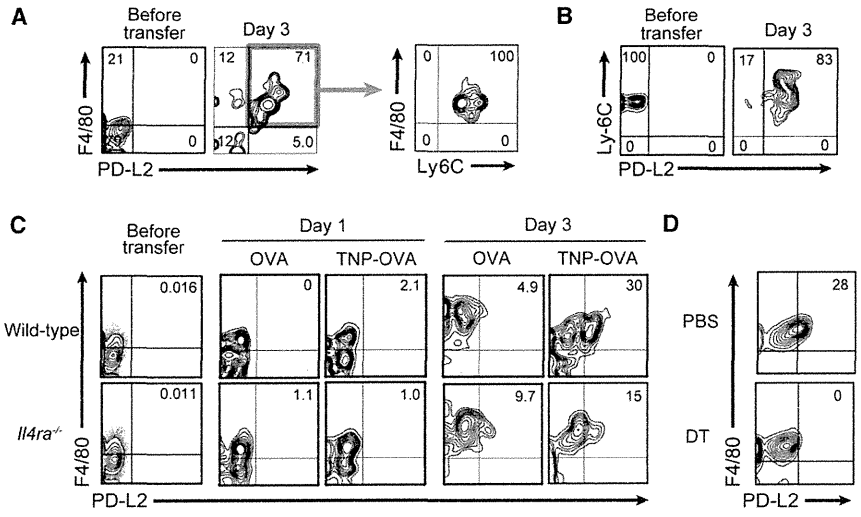

Figure 6. CD115$^+$ Monocytes Acquire PD-L2 Expression after Their Infiltration into the Skin Lesions, in a Manner Dependent on IL-4R and Basophils

(A and B) CD115$^+$ bone marrow cells isolated from BALB/c mice (A) or Ly6C$^+$Ly6G$^-$ inflammatory monocytes (purity > 99%) sorted from CD115$^+$ bone marrow cells (B) were labeled with CFSE and intravenously transferred (2 × 10^6 cells/mouse) into BALB/c mice that had been sensitized with anti-TNP IgE 1 day earlier. Recipient mice were challenged with intradermal administration of TNP-OVA immediately after the cell transfer. Flow cytometric analysis was performed for the surface expression of F4/80, PD-L2, and Ly6C in CFSE-labeled cells before the transfer and in those isolated from the TNP-OVA-injected skin on day 3 posttransfer.

(C) CD115$^+$ bone marrow cells were prepared from wild-type or *Il4ra*$^{-/-}$ mice, labeled with CFSE, and intravenously transferred (3 × 10^6 cells/mouse) into IgE-sensitized BALB/c mice, followed by the antigen challenge (TNP-OVA or control OVA) as in (A) and (B). Flow cytometric analysis was performed for the surface expression of F4/80 and PD-L2 in CFSE-labeled cells before the transfer (left) and in those isolated from the ear skin on day 1 and day 3 posttransfer (middle and right, respectively).

(D) *Mcpt8*^{DTR} C57BL/6 mice were sensitized with anti-TNP IgE and challenged with TNP-OVA as in Figure 1A to induce IgE-CAI. On day 2 postchallenge, the mice were treated with intravenous injection of CFSE-labeled CD115$^+$ bone marrow cells (1 × 10^7 cells/mouse) derived from wild-type mice, in conjunction with DT or control PBS. On day 4 postchallenge, the expression of F4/80 and PD-L2 on CFSE-labeled cells isolated from the ear skin was examined.

Data shown are representative of three independent experiments.

infection (Pesce et al., 2009). Notably, M2-like monocytes-macrophages infiltrating skin lesions of IgE-CAI express PD-L2, a ligand for the inhibitory receptor PD-1 (Loke and Allison, 2003). Blockade of PD-L2 with a specific antibody enhanced a Th2 cell-type response in helminth infection (Huber et al., 2010). However, our preliminary experiments with PD-L2 antibody suggested no apparent contribution of PD-L2 to the damping of allergic inflammation in IgE-CAI. In skeletal muscle injury, Ly6C$^+$ inflammatory monocytes are recruited and converted into "anti-inflammatory" macrophages that express IL-10 and transforming growth factor-β (TGF-β) (Arnold et al., 2007). In IgE-CAI, however, neither IL-10 nor TGF-β seems to be involved in damping inflammation in IgE-CAI (not all data shown). Of note, PD-L2$^+$ monocytes-macrophages accumulating in the IgE-CAI skin lesions expressed high amounts of a mannose receptor CD206 (Figure S6A), suggesting that they might have enhanced endocytic activity (Montaner et al., 1999). Indeed, PD-L2$^+$ monocytes-macrophages in the skin lesions showed a much higher extent of antigen uptake compared to PD-L2$^-$ monocytes-macrophages or other cell lineages including eosinophils and neutrophils (Figure S6B). This suggests that the failure in the generation of M2-like monocytes-macrophages may lead to the insufficient clearance of antigens in the skin lesions. Considering the fact that the extent and duration of the IgE-CAI reaction correlate well with the dose of antigens (Sato et al., 2003), the anti-inflammatory property of M2-like monocytes-macrophages could be attributed, at least in part, to their efficient uptake and clearance of antigens, making antigens unavailable for basophil activation.

Alternatively activated M2-type macrophages are typically generated by stimulation with the Th2 cell cytokines, IL-4 and IL-13, that can be produced by Th2 cells, natural killer T (NKT) cells, mast cells, eosinophils, basophils, and innate-type lymphoid cells (Paul and Zhu, 2010). Memory Th2 cells are the major source of Th2 cell cytokines for M2 generation in helminth infection (Anthony et al., 2006), whereas NKT cell-derived IL-4 is important for M2 generation in experimental autoimmune encephalomyelitis (Denney et al., 2012). In adipose tissues, eosinophil-derived IL-4 and IL-13 are crucial for M2 generation to maintain glucose homeostasis (Wu et al., 2011). In the present study, we demonstrated that basophil-derived IL-4 can act on inflammatory monocytes and convert them to anti-inflammatory M2-like monocytes-macrophages. Thus, basophils can contribute to the activation and differentiation of monocytes and macrophages, in addition to those of T and B cells as reported previously (Perrigoue et al., 2009; Sokol et al., 2008, 2009; Yoshimoto et al., 2009; Chen et al., 2009; Denzel et al., 2008). Of note, when stimulated ex vivo with IL-4, human CD14$^+$ monocytes display a phenotype characteristic for human M2-type macrophages, including upregulated expression of PD-L2 on their surface (Semnani et al., 2011). Given the fact that human basophils produce large quantities of Th2 cell cytokines as do murine basophils (Piccinni et al., 1991), it is plausible that basophils contribute to the generation of M2-type monocytes-macrophages in humans as observed in mice.

In conclusion, the present study demonstrated a previously unappreciated mode of monocyte-to-macrophage transition, that is, a conversion from inflammatory monocytes to anti-inflammatory M2-type monocytes-macrophages in an allergic response. In repeated infections with parasites, host animals often raise IgE against parasite antigens, and hence basophils can be stimulated with IgE plus antigens as seen in IgE-CAI (Karasuyama et al., 2011b; Voehringer, 2009). Moreover, basophils can be directly activated in an IgE-independent manner,

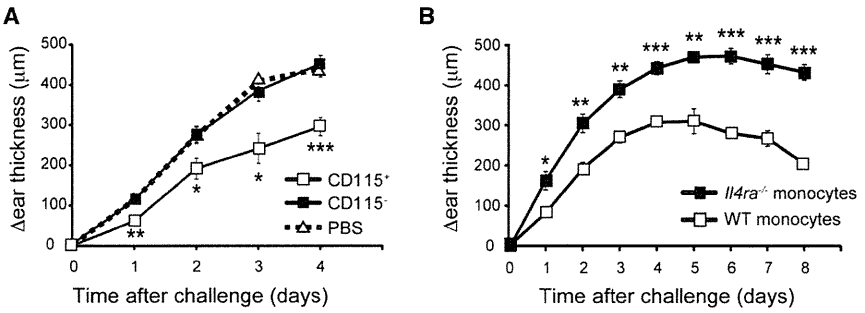

Figure 7. Adoptive Transfer of CCR2$^+$Ly6C$^+$ Inflammatory Monocytes from Wild-Type but Not *Il4ra*$^{-/-}$ Mice Normalizes the Exacerbated IgE-CAI in *Ccr2*$^{-/-}$ Mice

Ccr2$^{-/-}$ mice were treated as in Figure 3A to induce IgE-CAI.

(A) CD115$^+$ (open squares) or CD115$^-$ (closed squares) bone marrow cells from BALB/c mice or control PBS (open triangles) were intravenously administered to the mice four times (1 × 10^6 cells/injection/mouse), on days 0, 1, 2, and 3 post-challenge. Time course of ear swelling (Δear thickness) is shown (mean ± SEM, n = 3–5 each).

(B) Ly6C$^+$Ly6G$^-$ inflammatory monocytes (purity > 99%) sorted from bone marrow cells of wild-type (open squares) or *Il4ra*$^{-/-}$ (closed squares) mice were intradermally administered once (1 × 10^6 cells/site) in the ear of *Ccr2*$^{-/-}$ mice, in conjunction with administration of TNP-OVA or control OVA. Time course of ear swelling (Δear thickness) is shown (mean ± SEM, n = 4 each).

Data shown are representative of three independent experiments. *p < 0.05, **p < 0.01, ***p < 0.001. Note that error bars are displayed in all figures, but often are hidden behind symbols. See also Figures S6.

for example with certain proteases and pathogen products (Schroeder et al., 2001). Therefore, basophil-elicited M2 generation might be widely observed in various settings. Further studies will clarify their functional significance in each setting.

EXPERIMENTAL PROCEDURES

Mice

C57BL/6 and BALB/c mice were purchased from CLEA Japan. *Mcpt8*^{DTR} C57BL/6 (Wada et al., 2010), *Ccr2*$^{-/-}$ (Kuziel et al., 1997), and *Il4ra*$^{-/-}$ BALB/c (Noben-Trauth et al., 1997, 1999) mice were as described previously and maintained under specific-pathogen-free conditions in our animal facilities. All animal studies were approved by the Institutional Animal Care and Use Committee of Tokyo Medical and Dental University.

Induction of IgE-CAI

IgE-CAI was elicited as described previously (Mukai et al., 2005). In brief, mice were sensitized with intravenous injection of 300 μg of anti-TNP IgE, and on the following day challenged with an intradermal injection of 10 μg TNP_{12}-conjugated ovalbumin (OVA) and control OVA into the right and left ear, respectively. The value of Δear thickness, the differences in ear thickness (right − left) was calculated for the evaluation of inflammation.

Isolation of Bone Marrow Basophils and Monocytes

Basophils and monocytes were enriched from bone marrow cells via IMag system with biotinylated anti-CD49b and anti-CD115, respectively, followed by streptavidin-conjugated magnetic particles (BD PharMingen). Inflammatory monocytes were purified by sorting Ly6C^{hi}Siglec-F$^-$CD11c$^-$Ly6G$^-$ cells from the CD115$^+$ bone marrow cell population with FACSAria (BD Biosciences).

In Vitro Stimulation of Basophils and Monocytes

Basophils were stimulated for 10 hr with TNP_{12}-OVA or control OVA (300 ng/ml) after sensitization with TNP-specific IgE. The concentration of cytokines in culture supernatants was determined with Mouse IL-4 ELISA MAX Standard (Biolegend) for IL-4 and mouse Ready-Set-Go! ELISA kit (eBioscience) for IL-13. Monocytes were incubated for 24 hr with the culture supernatant of activated basophils in the presence or absence of anti-IL-4 or control rat IgG (20 μg/ml).

Ablation of Basophils

Mcpt8^{DTR} mice were treated once or twice with intravenous injection of diphtheria toxin (DT, Sigma-Aldrich, 500 ng/injection).

Statistical Analysis

Statistical analysis was performed with unpaired Student's t test. A p value <0.05 was considered statistically significant.

SUPPLEMENTAL INFORMATION

Supplemental Information includes Supplemental Experimental Procedures and six figures and can be found with this article online at http://dx.doi.org/10.1016/j.immuni.2012.11.014.

ACKNOWLEDGMENTS

We thank W.A. Kuziel (External Scientific Affairs, Daiichi Sankyo Group, Edison, NJ) for providing *Ccr2*$^{-/-}$ mice, D. Yamanaka and R. Matsunaga for technical support, and M. Miki for secretary assistance. This work was supported by a research grant from JST, CREST (to H.K.).

Received: August 4, 2012
Accepted: November 19, 2012
Published: February 21, 2013

REFERENCES

Anthony, R.M., Urban, J.F., Jr., Alem, F., Hamed, H.A., Rozo, C.T., Boucher, J.L., Van Rooijen, N., and Gause, W.C. (2006). Memory T(H)2 cells induce alternatively activated macrophages to mediate protection against nematode parasites. Nat. Med. *12*, 955–960.

Arnold, L., Henry, A., Poron, F., Baba-Amer, Y., van Rooijen, N., Plonquet, A., Gherardi, R.K., and Chazaud, B. (2007). Inflammatory monocytes recruited after skeletal muscle injury switch into antiinflammatory macrophages to support myogenesis. J. Exp. Med. *204*, 1057–1069.

Auffray, C., Fogg, D., Garfa, M., Elain, G., Join-Lambert, O., Kayal, S., Sarnacki, S., Cumano, A., Lauvau, G., and Geissmann, F. (2007). Monitoring of blood vessels and tissues by a population of monocytes with patrolling behavior. Science *317*, 666–670.

Auffray, C., Sieweke, M.H., and Geissmann, F. (2009). Blood monocytes: development, heterogeneity, and relationship with dendritic cells. Annu. Rev. Immunol. *27*, 669–692.

Biswas, S.K., and Mantovani, A. (2010). Macrophage plasticity and interaction with lymphocyte subsets: cancer as a paradigm. Nat. Immunol. *11*, 889–896.

Chen, K., Xu, W., Wilson, M., He, B., Miller, N.W., Bengtén, E., Edholm, E.S., Santini, P.A., Rath, P., Chiu, A., et al. (2009). Immunoglobulin D enhances immune surveillance by activating antimicrobial, proinflammatory and B cell-stimulating programs in basophils. Nat. Immunol. *10*, 889–898.

Denney, L., Kok, W.L., Cole, S.L., Sanderson, S., McMichael, A.J., and Ho, L.P. (2012). Activation of invariant NKT cells in early phase of experimental autoimmune encephalomyelitis results in differentiation of Ly6Chi inflammatory monocyte to M2 macrophages and improved outcome. J. Immunol. *189*, 551–557.

Denzel, A., Maus, U.A., Rodriguez Gomez, M., Moll, C., Niedermeier, M., Winter, C., Maus, R., Hollingshead, S., Briles, D.E., Kunz-Schughart, L.A.,